A stochastic agent-based model of pathogen propagation in dynamic multi-relational social networks

Bilal Khan[1], Kirk Dombrowski[2] and Mohamed Saad[3]

Abstract

We describe a general framework for modeling and stochastic simulation of epidemics in realistic dynamic social networks, which incorporates heterogeneity in the types of individuals, types of interconnecting risk-bearing relationships, and types of pathogens transmitted across them. Dynamism is supported through arrival and departure processes, continuous restructuring of risk relationships, and changes to pathogen infectiousness, as mandated by natural history; dynamism is regulated through constraints on the *local agency* of individual nodes and their risk behaviors, while simulation trajectories are validated using system-wide metrics. To illustrate its utility, we present a case study that applies the proposed framework towards a simulation of HIV in artificial networks of intravenous drug users (IDUs) modeled using data collected in the Social Factors for HIV Risk survey.

1 Introduction

Modeling the propagation of pathogens through risk-bearing interactions of actors in a social network is an emerging perspective in epidemiology, particularly in HIV research.[1–3] Approaches such as these shift our view of risk away from individuals to collective social bodies as the carriers and transmitters of infection. The subject of study here then is "risk networks", comprised of populations whose social interconnections signify particular "risk behaviors" that bear a potential for pathogen transmission. In the context of HIV, some examples of risk behaviors include social relationships which result in drug injection equipment sharing, and sexual relationships in the context of drug use. Although HIV will be used as a case study, the model presented in this paper is general enough to be applied towards the simulation of any epidemiological scenario in which disease transmission is driven by pairwise risk behaviors across a specifiable set of relationship types. Risk networks are now widely recognized as critical factors in understanding infection patterns, as they define the natural environment in which risk behaviors occur, and through which the propagation of infection proceeds.[4,5] The value of network-based simulation then, is that it can make the dynamic structures of risk visible and compelling,[6] and help further a change in perspective to one that sees collectivities (and

their respective forms and dynamics) as health actors with specific and identifiable structures of risk.

For reasons of cost, most risk network studies are relatively small in scale compared to the size of the overall communities they seek to understand. Even large-scale network studies manage to interview only a small portion of the ambient risk network; e.g. the study of Social Factors for HIV Risk (SFHR) conducted in Brooklyn, New York, in the early 1990s involved interviews with several hundred people[7] out of the 30,000–80,000 intravenous drug users (IDUs) in Brooklyn at the time. In contrast, simulation allows researchers to operate at the scale of the phenomenon of interest. While simulation is necessarily far from perfect and not a substitute for direct research, when based on detailed data and constructed to conform closely to known,

[1]Department of Math and Computer Science, John Jay College (CUNY), New York City, New York, USA
[2]Department of Sociology, University of Nebraska—Lincoln, Lincoln, Nebraska, USA
[3]NYC Social Network Research Group, John Jay College (CUNY), New York City, New York, USA

Corresponding author:
Bilal Khan, Deptartment of Math and Computer Science, John Jay College (CUNY), 524 W 59 St, New York, NY 10019, USA.
Email: bkhan@jjay.cuny.edu

short-term social dynamics, it can potentially provide suggestions and even tentative conclusions about critical health phenomenon at a time depth and social scale not possible in direct empirical research. Considerable prior work exists in which agent based modeling (ABM) is applied to questions of infectious disease epidemiology (see e.g. Nikolai and Madey for a recent review of ABM toolkits).[8]

Most previous ABM efforts consider spatial models wherein social networks are implicit through spatial proximity;[9–12] networks restructure themselves dynamically as actors move (coming in and out of pairwise contact). The EpiSimS system, for example, considers social contact to define a network over which the spread of pandemics may be explored via simulation.[13] Spatial contact-based stochastic agent models have also been used to study problems of infectious disease, including Enzootic Bovine Leukemia,[14] smallpox,[15] SARS,[16] and influenza.[17] ABM has even been used to evaluate the impact of the adoption of health care innovations,[18] and intervention strategy efficacies.[19] One strength of explicitly spatial approaches is that the micro-level movements/behaviors of individuals drive the simulation trajectory forward over time, and the parameters specifying these behaviors can be drawn from distributions that have been calibrated to *behavioral profile* data collected from the population modeled. A weakness of spatial models, however, is that *macro-level network characteristics*—e.g. degree distribution, and triangle prevalence or "transitivity" (the latter not preserved in Markov movement paradigms)—cannot be easily controlled through the course of the simulation without impinging on actor agency (though for recent progress relating spatial models with small-world network structure see Huang et al.).[20,21]

Exemplary research efforts to generate networks having specified macro-level characteristics include the work of Hamill and Gilbert,[22] wherein artificial networks are generated to mimic structural characteristics observed in real-world social networks (e.g. sparseness, short distances, searchability, fat tails, assortativeness, transitivity, and clustering). Such efforts are part of a long line of inquiry concerning the problem of generating random networks having the characteristics of social networks seen "in the wild"—see Watts and Strogatz, Barabasi and Albert, and Dorogovtsev and Mendes for example.[23–25] The problem of generating random *k*-regular graphs (i.e. the case where the degree distribution is uniform) has been the subject of a sequence of results starting with the work of Bender and Canfield,[26] the switching process of McKay and Wormald,[27] and the configuration model.[28,29] The more difficult problem of generating random graphs satisfying a specified univariate degree distribution (over all nodes), or bivariate degree distribution (over all edges) remains a subject of ongoing inquiry. Generally speaking, the unbalanced (power-law) degree sequences of social networks mandate the development of inhomogeneous random graph models.[30] The problem of efficiently generating networks

with a specific non-uniform degree *sequence* (across all nodes) is a well-known and difficult problem that has received considerable attention in recent years,[31–33] and the problem of generating graphs with a prescribed joint degree distribution has only been recently addressed by Stanton and Pinar using Markov chain techniques.[34]

Complicating matters further is the fact that the plausibility of an artificially generated social network rests on more than merely the extent to which its univariate and bivariate degree distributions reflect those observed in the real-world population being modeled. Many other aspects of network structure might influence the likelihood of edge formation. One such example arises when individual nodes are assumed to have associated attributes (e.g. gender), since then attribute homophily may exert a bias on edge likelihoods (e.g. if same gender or opposite gender links are more predominant in the population/relationship being modeled). Another example arises in the presence of small scale structural effects like transitivity (the bias to edges forming between two individuals who share a network neighbor). To determine the extent to which edge formation is influenced by phenomena such as attribute homophily or relation transitivity, one may employ the techniques of exponential random graph modeling (ERGM), which were originally put forth by Holland and Leinhardt and Frank and Strauss,[35,36] with estimation questions settled recently by Snijders et al.[37] ERGM models of networks can be used to generate artificial networks.[38–41] As described by Goodreau, such studies can also create dynamic networks where the connections between node actors are periodically reassigned according to a given distribution of pair-wise likelihoods.[42] As such, ERGM networks can be made to "evolve" over time, though at the cost of readily controllable actor agency. One strength of ERGM simulation models then is that *macro-level network characteristics* (e.g. the network's instantaneous degree distribution) drive the simulation trajectory over time, and these characteristics may be calibrated against measurements of the actual population being modeled. A weakness of ERGM simulation models, on the other hand, is that the micro-level behaviors of individuals (implicit in edge restructuring) cannot be readily controlled and made to reflect the known *behavioral profiles* exhibited in the population being modeled. Indeed, when discussing their future efforts, Snijders et al. refer to the need for "stochastic actor-based models for network dynamics".[43] As Snijders describes it, networks gain their dynamism as actors come and go from the network, and when they change their mutual connections due to:

> the structural positions of the actors within the network—e.g. when friends of friends become friends—characteristics of the actors ("actor covariates"), characteristics of pairs of actors ("dyadic covariates"), and residual random influences representing unexplained influences.[43:p.44]

What is needed is a framework in which *macro-level network characteristics* and individual micro-level *behavioral profiles* both play a role. Such a framework is developed and presented here, specifically for application towards the study of disease epidemiology. The framework is designed with the following guiding principles in mind:

- Like ABM-based simulations, we want to maintain an actor-based environment, where actions which determine network dynamism originate in characteristics of the nodes themselves. Such actor-based dynamism should include risk behaviors, length of network participation, and when and how to establish new network connections or get rid of prior ones.

- Like ERGM-based simulations, we want link creation to reflect node-specific attributes (such as gender, age, ethnicity/race), and local structural tendencies (e.g. network transitivity), so that our dynamic network remains "real-world viable" over long simulation trajectories, even while individual nodes/actors enter or leave the network.

- Like ABM-based simulations, we want our actors to exhibit individual behavior patterns (beyond node-specific characteristics such as age, or gender) parametrized from a distribution of possibilities, and to allow for different modalities of participation (such as one might see from two very different classes of network actors who are otherwise indistinguishable on the basis node characteristics).

- Like ERGM-based models, we want to be able to control for network-level factors affecting overall network dynamism, such as bounded deviation from a specific network-wide degree distribution.

- Like ABM-based simulations, we want to be able to simulate large networks, to determine whether factors of scale influence network dynamics and infection trajectories over simulation time, and to examine simulation results on a scale of the phenomena of interest.

Towards this, Marshall et al. have recently made progress by demonstrating an ABM approach that considers both macro-level network characteristics and individual micro-level behavioral profiles, in the context of their work on HIV interventions in IDU risk networks.[44] Of relevance also is recent work on the analysis of muti-relational networks,[45–47] and the simulation of such models of both online and real-world communities.[48,49]

In this paper we present a case study that extends the approach of Marshall et al.,[44] providing an illustrative application of our general-purpose framework for epidemiological modeling which considers multi-pathogen multi-layer networks by synthesizing both ERGM and ABM approaches. A more detailed comparison of features is given as part of the case study (see Section 5).

The framework is presented in stages. We begin, in Section 2, by considering static risk networks. First, in Section 2.1, we describe how a population survey can be used to obtain a description of a concrete real-world risk network, and how from this one may determine which attributes (of individuals) exert the greatest influence on the formation of risk relationships. In Section 2.2, we present the derivation of an (m, l, p) statistical network model—in effect, a distribution over the space of all *static* networks, which reflects the properties of the concrete risk network being modeled. In Section 2.3, we discuss how one may use a statistical network model to generate new (static) artificial risk networks. Finally, in Section 2.4, we address the need to validate generated artificial risk networks against the original real-world risk network from which the generative model was distilled. To simulate infection across these networks, the framework is extended in Section 3 to permit each of p distinct types of pathogens to flow between individuals via any of the l different types of risk relationships. Lastly, in Section 4, network dynamism is captured via node arrival and departure processes, incremental changes to individual risk relationship structures, and node aging. Finally, to illustrate the efficacy of the proposed framework, we apply it towards a case study of HIV in IDU communities where drug equipment sharing and sex in the context of drug use are the principal risk events underlying the transmission of HIV; the case study and associated simulation results are presented in Section 5.

Throughout this exposition, we adhere to certain notational conventions. Sets will be denoted by capital letters, A, B, C, etc., and will be indexed by integer variables i, j, k, etc. Elements within sets will be written in lower case Roman letters, a, b, c, etc. Distributions will usually be expressed as α, β, γ, etc. Types or proper names will be represented in script $\mathscr{A}, \mathscr{B}, \mathscr{C}$, etc. In an exposition where a set or function (e.g. the actors V) must be considered time-dependent, the temporal index will be *superior*, (causing us to write V^t for the set of actors at time t). In situations where a set or function (e.g. the infectiousness curve I) is being seen in the context of a particular layer, attribute, or pathogen type, this dependency will be made clear in the *subscript* of the variable (e.g. $I_{j,k}$ is the infectiousness curve of pathogen k via risk acts in layer j). Both superiors (for time) and inferiors (for context) will be employed simultaneously when referencing sets or functions that are both time and context dependent (e.g. $N_j^t(v)$ is the set of neighbors of actor v within network layer j at time t). A function f whose domain is D and range is R will be declared so by the statement $f : D \rightarrow R$. Set differences are indicated using the reverse solidus ($\backslash$) operator.

2 Modeling network structure

We view a risk network as an *l*-layer combinatorial fabric, weaving together a set of n individuals, each of whom has

m attributes, and may host one or more of p distinct types of pathogens. In what follows, we present how a real-world risk network is described (2.1), modeled statistically (2.2), and how the statistical network model can be subsequently used to sample new artificial risk networks (2.3) that can be validated against the original real-world network (2.4).

2.1 Obtaining data on real-world risk networks

In a survey of a population V, each constituent individual v is interrogated regarding a fixed set of m attributes $X = \{x_1, \ldots x_m\}$; e.g. x_1 could be gender, while x_2 might be age, and so on. We assume that each variable x_i (for $i = 1, \ldots, m$) is categorical, taking values from a finite set U_i that is known in advance (e.g. U_1 could be {Male, Female}, while U_2 might be {21AndUnder, Over21}). Each node attribute x_i ($i = 1, \ldots, m$) is seen as a function $x_i : V \to U_i$.

Yet to model a risk network, the survey must go beyond individual attributes and collect data on the risk relationships between them. The relationships of interest might be of several concrete types $\mathscr{T}_1, \mathscr{T}_2, \ldots, \mathscr{T}_l$. For example, $\mathscr{T}_1$ might be the relationship of "sharing injection equipment with", while $\mathscr{T}_2$ relationships could embody "sexual partnership", and so on. In practice, during the survey, each individual v from V is questioned about their risk relationships for each type $\mathscr{T}_j$ (for $j = 1, \ldots, l$), and is asked to provide sufficient information with which to identify the individuals $N_j(v) \subseteq V$ with whom v enjoys a type $\mathscr{T}_j$ relationship. In other words, the survey must be capable of capturing ego network data that, in turn, can be aggregated to produce a network whose structural features are representative of the topological characteristics of the risk network as a whole. The data thus collected is used to define a degree $d_j(v) \stackrel{\text{def}}{=} |N_j(v)|$ for each individual v; the value of this quantity is the number of type $\mathscr{T}_j$ relationships that v has. The set of all pairwise relationships, at each network *layer* $j = 1, \ldots, l$ is then expressible as $E_j = \bigcup_{v \in V} N_j(v)$.

Finally, the survey must produce data on the prevalence and distribution of the pathogens of interest, which may be of several distinct types $\mathscr{P}_1, \mathscr{P}_2, \ldots, \mathscr{P}_p$. Specifying the instantaneous state of a risk network thus requires a collection of p concrete sets of individuals $A_1, A_2, \ldots, A_p \subseteq V$ where A_k is the set of individuals who are positive for pathogen type $\mathscr{P}_k$ ($k = 1, 2, \ldots, p$).

Collecting the above elements, we define a **risk network** to be an $(m + 2l + p + 1)$ tuple $\mathcal{D} \stackrel{\text{def}}{=} (x_i, V, E_j, A_k, d_j)$ where $i = 1, \ldots, m; j = 1, \ldots, l; k = 1, \ldots, p$.

2.2 Defining a statistical network model

In modeling a risk network $\mathcal{D}$, the question arises as to the contents of the model, and particularly, which m attributes $X = \{x_1, \ldots x_m\}$ to consider. Questions of determinate variables (and their relative importance), are of paramount importance to our modeling process. In particular, we need to determine which individual attributes were important to the formation of the network, and to know how these attributes rank relative to one another.

Recently, the statistical analysis of network data has been advanced considerably by the introduction of ERGM, which provides researchers with an alternative to the simple cross-tabulation of network link data. ERGM is a statistical technique aimed at determining the extent to which the likelihood of network linkages appears to be biased towards (or against) the creation of specified network substructures, above and beyond what is expected by chance occurrence. Such substructures can be as simple as the tendency of "like" nodes to be connected (at a greater rate than expected by a random distribution of connections), or as complex as specific structures of connection between several individuals.[50] The theoretical basis for ERGM analysis was laid down by Holland and Leinhardt and Frank and Strauss,[35,36] with estimation questions finally settled only recently.[37] Readers can find a detailed exposition of ERGM in Goodreau, Goodreau et al., and Kolaczyk.[38–40]

To begin the process of parameterizing the models, we apply ERGM analysis to the data set $\mathcal{D}$ obtained from the survey. The outcome of such analysis is the m most influential attributes $X = \{x_1, \ldots x_m\}$, together with weights that quantify their relative influence. In addition, we use ERGM to evaluate the influence of significant network substructures. These can be as simple as edge reciprocity or network transitivity, or as complex as those discussed by Bearman et al.[50] Here we consider only the influence of triadic closure (i.e. transitivity) on link formation in each of the l network layers; these l weights are denoted w_j^Δ (for $j = 1, \ldots, l$). Triadic closure was found to be in the SFHR network data on which the case study of our framework is based. SFHR considered risk relationships between intravenous drug users which were based on equipment co-use, and the stigmatized nature of the pairwise relationships clearly leads to a bias towards triad formation (if A co-uses with B and C, then B and C are more likely to co-use together). In other networks, such as those where the edge relation signifies sexual intercourse, no bias towards transitivity is seen. (In general, social network analysis has revealed the importance of both link reciprocity (where an edge in a single direction is likely to be matched by a return edge at a higher rate than expected at random) and network transitivity (where structural holes between two vertices, each with an edge to a common third party but who are not themselves connected by by an edge, occur at a lesser rate than expected at random). In the case of risk networks, where relationships and the events they facilitate are necessarily bi-directed, reciprocity is assumed for all edges. As such, only transitivity is considered here, though we note that ERGM analysis is

capable of providing model weights for any network sub-structure of interest.)

Attribute distributions. Given a risk network $\mathcal{D} = (x_i, V, E_j, A_k, d_j)$ where $i = 1, \ldots, m$; $j = 1, \ldots, l$; $k = 1, \ldots, p$, we can from each of the attributes x_i ($i = 1, \ldots, m$), determine a **univariate attribute distribution** $\alpha_i : U_i \to [0, 1]$ for $i = 1, 2, \ldots, m$, where for $u \in U_i$,

$$\alpha_i(u) \stackrel{\text{def}}{=} \frac{1}{|V|} |x_i^{-1}(u)|$$

If a chi-squared test reveals a significant level of association to be present between α_i and $\alpha_{i'}$ (for $i \neq i'$), then the categorical attribute variables x_i and $x_{i'}$ are coalesced into a new joint variable x^* defined over the Cartesian product of categorical spaces $U_i \times U_{i'}$. The joint distribution α^* over a suitably binned $U_i \times U_{i'}$ is used whenever we need to sample a pair of values $(x_i, x_{i'})$. In this manner, we may inductively coalesce all attributes which show significant pairwise dependencies. Given this strategy, in what follows we simplify the exposition by assuming that $\{\alpha_i \mid i = 1, \ldots, m\}$ is a set of pairwise independent distributions.

Next, each set of type-$\mathcal{T}_j$ relationships E_j (for $j = 1, 2, \ldots, l$) is used to define a **bivariate attribute distribution** $\beta_{i,j} : U_i \times U_i \to [0, 1]$ for $i = 1, 2, \ldots, m$, where for each $u_1, u_2 \in U_i$,

$$\beta_{i,j}(u_1, u_2) \stackrel{\text{def}}{=} \frac{1}{|E_j|} |(x_i^{-1}(u_1) \times x_i^{-1}(u_2)) \cap E_j|$$

Degree distributions. Next, we model the layer-j degree distribution for the population, taking care to account for the fact that individual attributes and degrees are often related.(For example, maybe 20 year old Caucasian males consistently exhibit higher degrees than 40 year old African American females.) To capture this, we determine a suitable partition of the Cartesian product of the categorical spaces U_i ($i = 1, \ldots, m$)

$$\mathcal{C}_1^j \sqcup \mathcal{C}_2^j \sqcup \ldots \sqcup \mathcal{C}_s^j \sqcup \ldots \sqcup \mathcal{C}_{S_j}^j = \prod_{i=1}^{m} U_i$$

Informally, each of the $\mathcal{C}_s^j$ ($s = 1, \ldots, S_j$) represents a distinct class of individuals, where classes are differentiated from one another because they exhibit different'' ideal layer-j degree'' distributions. In practice, the value of S_j and the definition of each class $\mathcal{C}_s$ ($s = 1, \ldots, S_j$) is determined by performing a statistical analysis to discover which univariate attributes appear to significantly influence vertex degree (in layer j). From the results of such an analysis, classes are suitably defined so that the individuals within a single class can be assumed to draw their ideal layer-j degree from a distribution that is independent of their individual attribute values.

Since the set $\{\mathcal{C}_s^j \mid s = 1, \ldots, S_j\}$ is a partition of $\prod_{i=1}^{m} U_i$, and every $v \in V$ has attributes $(x_1(v), x_2(v), \ldots, x_m(v))$ which lie in exactly one of the S_j classes, we obtain a natural classification function $f_j^{\mathcal{C}} : V \to \{1, 2, \ldots, S_j\}$. Given such a classification function, the individuals V in a risk network can be naturally partitioned by class:

$$V(\mathcal{C}_1^j) \sqcup V(\mathcal{C}_2^j) \sqcup \ldots \sqcup V(\mathcal{C}_s^j) \sqcup \ldots \sqcup V(\mathcal{C}_{S_j}^j) = V$$

where $V(\mathcal{C}_s^j) \stackrel{\text{def}}{=} \{v \in V \mid f_j^{\mathcal{C}}(v) = s\}$

Each layer-j degree class $\mathcal{C}_s$ ($s = 1, \ldots, S_j$) exhibits its own **univariate degree distribution** $\chi_{j;s} : \mathbb{Z} \times \mathbb{Z} \to \mathbb{R}$ where for every pair of integers $a < b$, and $s \in \{1, \ldots, S_j\}$:

$$\chi_{j;s}(a, b) \stackrel{\text{def}}{=} \frac{|\{v \in V(\mathcal{C}_s^j) \mid a \leqslant d_j(v) < b\}|}{|V(\mathcal{C}_s^j)|}$$

In general, the layer-j degree distributions $\chi_{j;s}(a, b)$ for different classes s may differ from one another, and may differ from the overall "class-neutral" layer-j degree distribution

$$\chi_{j;*}(a, b) \stackrel{\text{def}}{=} \frac{|\{v \in V \mid a \leqslant d_j(v) < b\}|}{|V|}$$

If a chi-squared test reveals a significant level of association to be present between the class-neutral degree distributions of two layers, say $\chi_{j;*}$ and $\chi_{j';*}$ (for $j \neq j'$), then the degree distributions of the two layers j and j' must be coalesced into a new joint variable χ^* over the Cartesian product $\mathbb{N} \times \mathbb{N}$, using a common refinement of the classification schemes $\{\mathcal{C}_s \mid s = 1, \ldots, S_j\}$ and $\{\mathcal{C}_s' \mid s = 1, \ldots, S_{j'}\}$. The distribution χ^* is used to simultaneously sample a pair of degrees (for network layers j and j'). In this manner, we may (for the purpose of degree sampling) inductively coalesce all network layers which show significant pairwise dependency in their degree distributions. Given this strategy, without loss of generality, in what follows we simplify the exposition by assuming that the set $\{\chi_{j;*} \mid j = 1, \ldots, l\}$ consists of pairwise independent distributions. The degree distribution in layer j is captured by the set of pairs

$$\mathbb{X}_j \stackrel{\text{def}}{=} \{(\mathcal{C}_s^j, \chi_{j;s}) \mid s = 1, 2, \ldots, S_j\}$$

which functionally specifies a distribution for each of the classes in $\{\mathcal{C}_s \mid s = 1, \ldots, S_j\}$.

For each $j = 1, \ldots, l$ we also define a **bivariate degree distribution** $\bar{\bar{\chi}}_j : (\mathbb{Z} \times \mathbb{Z})^2 \to \mathbb{R}$ where for every 4-tuple of integers $a < b, a' < b'$

$$\bar{\bar{\chi}}_j(a, b, a', b') \stackrel{\text{def}}{=}$$

$$\frac{|\{e \in E_j \mid e = (u, v); a \leqslant d_j(u) < b; a' \leqslant d_j(v) < b'\}|}{|E_j|}$$

Pathogen distributions. For each of the p pathogen types $\mathscr{P}_k$ ($k = 1, 2, \ldots, p$), we model its *prevalence*, taking care to account for the fact that individual attributes and pathogen prevalences are often related.(For example, perhaps 20 year old Caucasian males consistently exhibit lower HIV prevalence than 40 year old African American females.) To capture this, we determine a suitable partition of the Cartesian product of the categorical spaces U_i ($i = 1, \ldots, m$)

$$\mathcal{B}_1^k \sqcup \mathcal{B}_2^k \sqcup \ldots \sqcup \mathcal{B}_r^k \sqcup \ldots \sqcup \mathcal{B}_{R_k}^k = \prod_{i=1}^{m} U_i$$

Informally, each of the $\mathcal{B}_r^k$ ($r = 1, \ldots, R_k$) represents a distinct class of individuals, where classes are differentiated from one another because they exhibit different"-pathogen-k prevalence" levels. In practice, the value of R_k and the definition of each class $\mathcal{B}_r$ ($r = 1, \ldots, R_k$) is determined by performing a statistical analysis to discover which univariate attributes appear to significantly influence pathogen prevalence (with respect to pathogen k). From the results of such an analysis, classes are suitably defined so that the individuals in a single class can be assumed to draw their pathogen-k infection status via a Bernoulli trial whose outcome is positive with a constant probability that is independent of the individual's attributes.

Since the set $\{\mathcal{B}_r \,|\, r = 1, \ldots, R_k\}$ is a partition of $\prod_{i=1}^{m} U_i$, and every $v \in V$ has attributes $(x_1(v), x_2(v), \ldots, x_m(v))$ which lie in exactly one of the R_k classes, we obtain a natural classification function $f_k^{\mathcal{B}} : V \to \{1, 2, \ldots, R_k\}$. Given such a classifying function, the individuals V in a risk network may be partitioned by class:

$$V(\mathcal{B}_1^k) \sqcup V(\mathcal{B}_2^k) \sqcup \ldots \sqcup V(\mathcal{B}_r^k) \sqcup \ldots \sqcup V(\mathcal{B}_{R_k}^k) = V$$

where $V(\mathcal{B}_r^k) \stackrel{\text{def}}{=} \{v \in V \,|\, f_k^{\mathcal{B}}(v) = r\}$.

Each pathogen-k prevalence class $\mathcal{B}_r$ ($r = 1, \ldots, R_k$) exhibits its own **pathogen prevalence** $p_{k;r} \in \mathbb{R}$ where for every $k = 1, 2, \ldots, p$, and $r \in \{1, \ldots, R_k\}$:

$$p_{k;r} \stackrel{\text{def}}{=} \frac{|A_k \cap V(\mathcal{B}_r^k)|}{|V(\mathcal{B}_r^k)|}$$

where

$$A_k \stackrel{\text{def}}{=} \{v \in V \,|\, v \text{ is positive for pathogen } k\}.$$

The prevalence of pathogen k is captured by the set of pairs

$$\mathbb{P}_k \stackrel{\text{def}}{=} \{(\mathcal{B}_r^k, p_{k;r}) \,|\, r = 1, 2, \ldots, R_k\}$$

which functionally specifies a distribution for each of the classes in $\{\mathcal{B}_r \,|\, r = 1, \ldots, R_k\}$.

The **statistical network model** $\mathcal{M}(\mathcal{D})$ of risk network $\mathcal{D}$ is the $(m + (m+2)l + p)$-tuple:

$$\mathcal{M}(\mathcal{D}) \stackrel{\text{def}}{=} (\alpha_i, \beta_{i,j}, \mathbb{X}_j, \bar{\bar{\chi}}_j, \mathbb{P}_k)_{i=1,\ldots,m; j=1,\ldots,l; k=1,\ldots p}$$

2.3 Generating networks from a statistical network model

Given a statistical network model $\mathcal{M}$, procedure **MakeNetwork** (Algorithm 1) instantiates a new artificial risk network of size n, using $\mathcal{M}$ as a statistical guideline.

In the first phase (line 1 of Algorithm 1), the **MakePopulation** procedure is called (Algorithm 2), which in turn, creates n individuals, assigning each of their m attributes independently at random, using the univariate distributions $\alpha_1, \ldots, \alpha_m$ (lines 4,5). Then (lines 7–10) the degree distributions $\mathbb{X}_j$ are used to assign each individual an ideal ego network size, or **ideal degree**, $d_j(v)$, based on v's ideal layer-j degree class s, for each of the layers $j = 1, \ldots, l$. Justification for individuals having an intrinsic ideal degree comes from prior work on the emergence of "roles" within risk networks.[51–53]

In the second phase (line 2 of Algorithm 1), the **MakePathogens** procedure is called (see Algorithm 3), which in turn, distributes each of the p types of pathogens (line 2) to each of the individuals in V (line 3), in a manner that reflects the specified prevalence levels for the particular pathogen type (lines 4–7), based on v's pathogen-k prevalence class t, for each of the pathogen $k = 1, \ldots, p$.

In the third phase (line 3 of Algorithm 1), the **MakeRelations** procedure creates risk relationships between individuals (see Algorithm 4). To do this, it initializes the layer j neighbors (line 3) of each node v_i (line 2) to be the empty set (line 4), and then schedules $d_j(v_i)$

Algorithm 1: Procedure **MakeNetwork**

    Input: statistical network model $(\alpha_i, \beta_{i,j}, \mathbb{X}_j, \bar{\bar{\chi}}_j, \mathbb{P}_k)_{i=1,\ldots,m; j=1,\ldots,l; k=1,\ldots,p}$; population size n

    Output: risk network $(x_i, V, E_j, A_k, d_j)_{i=1,\ldots,m; j=1,\ldots,l; k=1,\ldots,p}$

1 $(\{x_i\}, \{d_j\}, V) \leftarrow$ **MakePopulation**$(n, \{\alpha_i\}, \{\mathbb{X}_j\})_{i=1,\ldots,m; j=1,\ldots,l}$

2 $\{A_k\} \leftarrow$ **MakePathogens**$(V, \{\mathbb{P}_k\})_{k=1,\ldots,p}$

3 $E \leftarrow$ **MakeRelations**$(\{\beta_{i,j}\}, \{\bar{\bar{\chi}}_j\}, \{x_i\}, \{d_j\}, V)_{i=1,\ldots,m; j=1,\ldots,l}$

4 **return** $(x_i, V, E_j, A_k, d_j)_{i=1,\ldots,m; j=1,\ldots,l; k=1,\ldots,p}$

Algorithm 2: Procedure **MakePopulation**

  Input: population size n, attribute distributions $\{\alpha_i\}_{i = 1, ..., m}$, degree distributions $\{\mathbb{X}_j\}_{j = 1, ..., l}$

  Output: $(\{x_i\}, \{d_j\}, V)_{i = 1, ..., m; j = 1, ..., l}$

1   $V = \{v_1, v_2, \ldots, v_n\}$

2   **foreach** v_k *in* V **do**

3   // Set the attributes of individual v_k.

4   **foreach** i *in* $1, \ldots, m$ **do**

5          $x_i(v_k) :=$ an element of U_i randomly selected via α_i.

6   // Set individual v_k's ideal ego net size at each layer.

7   **foreach** j *in* $1, \ldots, l$ **do**

8          $s := f_j^{\mathcal{C}}(v)$, the layer-$j$ ideal degree class of v_k.

9          $\tau := \chi_{j;s}$ the corresponding layer-j ideal degree distribution, taken from $Range(\mathbb{X}_j)$.

10        $d_j(v_k) :=$ an integer randomly chosen via pdf τ.

11 **return** $(\{x_i\}, \{d_j\}, V)_{i = 1, ..., m; j = 1, ..., l}$

Algorithm 3: Procedure **MakePathogens**

  Input: population V, pathogen prevalences $\{\mathbb{P}_k\}_{k = 1, ..., p}$

  Output: $\{A_k\}_{k = 1, ..., p}$

1   $A_1 = A_2 = \ldots = A_p = \emptyset$

2   **foreach** k *in* $1, \ldots, p$ **do**

3   **foreach** v_i *in* V **do**

4          $t := f_k^{\mathcal{B}}(v)$, identifying the pathogen-k class of v_i in $Domain(\mathbb{P}_k)$.

5          $\tau := p_{k;t}$ the corresponding pathogen-k prevalence rate in $Range(\mathbb{P}_k)$.

6   **if** $Random(0, 1) < \tau$ **then**

7             $A_k := A_k \cup \{v_i\}$

8   **return** $\{A_k\}_{k = 1, ..., p}$

Algorithm 4: Procedure **MakeRelations**

  Input: bivariate attribute distributions $\{\beta_{i,j}\}_{i = 1, ..., m; j = 1, ..., l}$, bivariate degree distributions $\{\bar{\bar{\chi}}_j\}_{j = 1, ..., l}$, individual attributes $\{x_i\}_{i = 1, ..., m}$ and ideal degrees $\{d_j\}_{j = 1, ..., l}$, the population V

  Output: E

1   $E = \emptyset$

2   **foreach** i *in* $1, \ldots, |V|$ **do**

3   **foreach** $j = 1, \ldots, l$ **do**

4          $N_j(v_i) := \emptyset$.

5   **foreach** $e = 1, \ldots, d_j(v)$ **do**

6   Schedule **AddEdge**(v_i, j) to take place at time $\frac{1}{ei + 1}$.

7   Wait until time 1.

8   $E := \bigcup_{i = 1}^{|V|} \bigcup_{w \in N(v_i)} \{(v, w)\}$

9   **return** E

Algorithm 5: procedure **AddEdge**.

   Input: individual v, layer j.

1 // Determine candidate new neighbors for v.

2 $C_j^t(v) := V_j^t \backslash (N_j^t(v) \cup \{v\})$

3 **if** $|C_j^t(v)| > 0$ **then**

4   **foreach** c in $C_j^t(v)$ **do**

5   Compute the bias due to degree constraints:

$$a_\delta^t(c) := \begin{cases} e^{-1/(d_j(v) - |N_j^t(v)|)} & |N_j^t(u)| < d_j(u) \\ 0 & \text{otherwise} \end{cases}$$

6   Compute the bias due to the bivariate degree distribution:

$$a_\chi^t(v, c) := \bar{\bar{\chi}}_j(|N_j^t(v)| - \epsilon, |N_j^t(v)| + \epsilon, |N_j^t(c)| - \epsilon, |N_j^t(c)| + \epsilon)$$

7   Compute the bias due to bivariate attribute distributions:

$$a_\beta^t(c) := \prod_{i=1}^{m} \beta_{i,j}(x_i(v), x_i(c))$$

8   Compute the bias due to triadic closures:

$$a_\Delta^t(c) := (w_j^\Delta - 1) \cdot \Delta_j^t(v, c)$$

      where $\Delta_j^t(v, c) = $ # layer j triangles formed on adding layer j edge (v, c).

9   Compute propensity of edge (v, c) as the product of four biases:

$$\omega_j^t(c) := a_\delta^t(c) \cdot a_\chi^t(c) \cdot a_\alpha^t(c) \cdot a_\Delta^t(c)$$

10   Normalize propensity to obtain a distribution over $C_j^t(v)$:

$$p_j^t(c) := \frac{\omega_j^t(c)}{\sum_{c' \in C_j^t(v)} \omega_j^t(c')}$$

11 $w :=$ choose from $C_j^t(v)$ randomly according to distribution p_j^t.

12 // Add the layer j edge connecting v to w.

13 $N_j^t(v) := N_j^t(v) \cup \{(v, w)\}$

---

executions of **AddEdge** for each node v_i at each layer j (lines 5,6). Because all calls to **AddEdge** are at times < 1, **MakeRelations** need only wait until time 1 before aggregating the set of all edges (line 8).

Each execution of **AddEdge** is in the context of a given vertex v, layer j, and time t (Algorithm 5). The procedure first computes the set $C_j^t(v)$ of candidate new layer-j neighbors of v (line 2), proceeding only if this is nonempty (line 3). It then (a) computes the layer j edge deficit for each candidate vertex c (line 5), taking this to be the difference between v's ideal degree $d_j(v)$ and actual degree $|N_j^t(v)|$, rescaled into the interval $[0, 1]$ by composing with the smooth squashing function $e^{\frac{-1}{x}}$. The squashing function

approaches 1 as $x \to \infty$ and 0 as $x \to 0^+$. The quantity $a_\delta(c)$ is thus close to 1 whenever $|N_j^t(c)| \ll d_j(c)$ and becomes 0 once c's actual degree $|N_j^t(c)|$ attains its ideal value $d_j(c)$. The selection of candidate c is also influenced by (b) the actual degrees of v and c (line 6), with respect to the bivariate degree distribution $\bar{\bar{\chi}}_j$ (suitably binned to 2ϵ-sized buckets). Likewise (c) the joint attributes of v and c influence the candidate selection (line 7), reflecting the bivariate attribute distributions $\beta_{i,j}$. Finally, (d) each new triangle arising from the addition of edge (v, c) contributes $(w_j^\Delta - 1)$ to the total triadic bias (line 8) which is accumulated in $a_\Delta^t(c)$. The factors (a)–(d) are used to construct a probability distribution p_j^t over the set of candidate new

layer-j neighbors (lines 9,10), using which one of the candidates w is selected (line 11). The edge (v, w) is then added to network layer j by augmenting the set of layer j edges emanating from v (line 13).

2.4 Validating generated networks

We have shown how, from a network survey, one may specify a real-world risk network $\mathcal{D}$ (see Section 2.1), and from $\mathcal{D}$ derive a statistical network model $\mathcal{M}$ (see Section 2.2), and then use the model $\mathcal{M}$ to sample new artificial risk networks $\mathcal{D}'_1, \mathcal{D}'_2, \mathcal{D}'_3, \ldots$ (see Section 2.3). We now present techniques to quantify the divergence between the original real risk network $\mathcal{D}$ and a generated artificial risk network(s) $\mathcal{D}'$. These techniques shall be particularly relevant to assessing the possible **degeneracy** of model $\mathcal{M}$, i.e. its potential inability to generate networks that reflect characteristics of the network from which the model was derived.

We begin by considering how one may measure the similarity or difference between two (m, l, p) statistical network models

$$\mathcal{M}_1 = (\alpha_i, \beta_{i,j}, \mathbb{X}_j, \bar{\bar{\chi}}_j, \mathbb{P}_k)_{i = 1, \ldots, m; j = 1, \ldots, l; k = 1, \ldots, p}$$
$$\mathcal{M}_2 = (\alpha'_i, \beta'_{i,j}, \mathbb{X}'_j, \bar{\bar{\chi}}'_j, \mathbb{P}'_k)_{i = 1, \ldots, m; j = 1, \ldots, l; k = 1, \ldots, p}$$

Because $\mathcal{M}_1$ and $\mathcal{M}_2$ each consist of a set of distributions, the two models are readily comparable only if the domains of these distributions agree. In particular, for two models to be comparable it is necessary that

$$Domain(\alpha_i) = Domain(\alpha'_i)$$
$$Domain(\beta_{i,j}) = Domain(\beta'_{i,j})$$

for all $i = 1, \ldots, m; j = 1, \ldots, l$. Likewise, the set of ideal layer-j degree classes (referred to via $\mathbb{X}_j$ and $\mathbb{X}'_j$), and pathogen-k prevalence classes (referred to via P'_k and P'_k) must be compatible:

$$Domain(\mathbb{X}_j) = Domain(\mathbb{X}'_j)$$
$$Domain(\mathbb{P}_k) = Domain(\mathbb{P}'_k)$$

for all $j = 1, \ldots, l; k = 1, \ldots, p$. The above conditions can be met by any pair of (m, l, p) statistical network models by using a suitable common refinement of the categorical spaces U_i and U'_i (for $i = 1, \ldots, m$), classifications $\mathbb{X}_j, \mathbb{X}'_j$ (for $j = 1, \ldots, l$), and $\mathbb{P}_k, \mathbb{P}'_k$ (for $k = 1, \ldots, p$).

Given two comparable models how might one quantify their similarity or difference?

Since statistical network models are tuples of distributions, we begin by considering how one may assess the similarity between two probability distributions f, f' over a common set X. Many approaches exist, including histogram intersection,[54] chi-square statistics,[55] quadratic form distance, match distance, Kolmogorov–Smirnov distance,[56] earth mover's distance, Kullback–Leibler divergence—sometimes now called information divergence, information gain, or relative entropy—[57] and Jensen–Shannon divergence—also known as information radius or IRad. Here we shall chose to measure the difference between two probability distributions as

$$\Delta(f, f') \overset{\text{def}}{=} \sqrt{\text{IRad}(f, f')}$$

because by doing so, we obtain a metric space on the set of all probability distributions over an underlying set. [58,59] The IRad of two distributions is defined to be their mean Kullback–Leibler divergence from their average (as distributions). Applying this to the constituent distributions in the two models, we get

$$\Delta(\alpha_i, \alpha'_i) \overset{\text{def}}{=}$$
$$\sqrt{\sum_{x \in U_i} \alpha_i(x) \log \frac{\alpha_i(x)}{\bar{\alpha}_i(x)} + \alpha'_i(x) \log \frac{\alpha'_i(x)}{\bar{\alpha}_i(x)}}$$

$$\Delta(\beta_{i,j}, \beta'_{i,j}) \overset{\text{def}}{=}$$
$$\sqrt{\sum_{(x,y) \in U_i \times U_i} \beta_{i,j}(x,y) \log \frac{\beta_{i,j}(x,y)}{\bar{\beta}_{i,j}(x,y)} + \beta'_{i,j}(x,y) \log \frac{\beta'_{i,j}(x,y)}{\bar{\beta}_{i,j}(x,y)}}$$

where $\bar{\alpha}_i$ is the average of α_i and α'_i (as a distribution over U_i), and $\bar{\beta}_{i,j}$ is the average of $\beta_{i,j}$ and $\beta'_{i,j}$ (as a distribution over $U_i \times U_i$). Analogous distance measures may be defined between the two models' bivariate degree distributions $\bar{\bar{\chi}}_j$ and $\bar{\bar{\chi}}'_j$, as well as between corresponding in-class univariate degree distributions $\chi_{j;s}$ and $\chi'_{j;s}$ (taken from $\mathbb{X}_j$ and $\mathbb{X}'_j$, respectively). Because these distributions are defined over identical partitions $\{\mathcal{C}^j_s \mid s = 1, \ldots, S_j\}$ of $\prod_{i=1}^m U_i$, we can aggregate the distances by summing the divergences between corresponding class distributions:

$$\Delta(\mathbb{X}_j, \mathbb{X}'_j) \overset{\text{def}}{=} \sum_{s = 1}^{S_j} \Delta(\chi_j, \chi'_j)$$

Having defined the distance between corresponding distributions in the two models, we use the L_∞ norm to extend to a definition of **distance between statistical network models**:

$$\Delta^*(\mathcal{M}_1, \mathcal{M}_2) \overset{\text{def}}{=}$$
$$\max\left(\max_{i=1}^m \Delta(\alpha_i, \alpha'_i), \quad \max_{j=1}^l \max_{i=1}^m \Delta(\beta_{i,j}, \beta'_{i,j}), \right.$$
$$\left. \max_{j=1}^l \Delta(\mathbb{X}_j, \mathbb{X}'_j), \quad \max_{j=1}^l \Delta(\bar{\bar{\chi}}_j, \bar{\bar{\chi}}'_j) \right) \qquad (1)$$

By considering the worst-case divergences of all constituent distributions within the two models, we hope to produce a holistic assessment of the relative validity of each model against the other.[60]

The **distance between** two **risk networks** $\mathcal{D}$ and $\mathcal{D}'$ (which have comparable models), is now taken as

$$\Delta(\mathcal{D}, \mathcal{D}') \stackrel{\text{def}}{=} \Delta^*(\mathcal{M}(\mathcal{D}), \mathcal{M}(\mathcal{D}')) \qquad (2)$$

Note that by not incorporating divergences of pathogen prevalence rates p_k (interpreted as Bernoulli distribution parameters) into the definition of Δ^*, we ensure that $\Delta(\mathcal{D}, \mathcal{D}')$ measures the extent to which $\mathcal{D}, \mathcal{D}'$ differ as networks; the pathogen prevalence rates in the two risk networks $\mathcal{D}, \mathcal{D}'$ may diverge arbitrarily without influencing the value of $\Delta(\mathcal{D}, \mathcal{D}')$.

We have thus transformed the set of all risk networks generated from comparable statistical network models into a metric space in which distance is inverse to similarity in network structure. In practice, the metric Δ (on risk networks) will allow us to detect when an (artificial) generated network $\mathcal{D}'$ is very different from the surveyed (real-world) risk network $\mathcal{D}$ from which the generative statistical network model $\mathcal{M}(\mathcal{D})$ was defined. By using rejection sampling[61] we may ensure that the artificial networks which are used as starting points of our simulation are not exceptionally different from the real-world networks from which our statistical network models are derived.

In the context of dynamic network simulation (to be described), Δ will allow us to keep track of the extent of structural divergence between the initial artificial risk network $\mathcal{D}'$ and its instantaneous evolute $\mathcal{D}'_t$ at time t (over the course of the simulation trajectory). If at some point (in time) in the simulation trajectory, we discover that $\mathcal{D}'$ and $\mathcal{D}'_t$ are significantly different (i.e. $\Delta(\mathcal{D}', \mathcal{D}'_t)$ exceeds some prescribed threshold), the definition of Δ permits us to dissect the contributions of the constituent distributions in $\mathcal{M}(\mathcal{D}'_t)$ and $\mathcal{M}(\mathcal{D}')$ to determine what aspects of the models are most responsible for the divergence. In such circumstances, either the trajectory can be discarded (because it has produced an exceptional network)—a form of rejection sampling from the space of all system trajectories; or, alternatively, the dynamism model parameters (to be described) may be altered to allow less drift in the risk network's structure over time.

Next, in Section 3, we shall extend the model to support pathogen dynamics. Then, in Section 4, we extend it further to capture the dynamic evolution of network topologies.

3 Modeling pathogens: The risk process

An individual v's infection status may change with respect to a pathogen $\mathcal{P}_k$ (for some k in $1, \ldots, p$) when v engages in risk behaviors (via layer j relationships, $j = 1, \ldots, l$) with a risk partner w who is positive for $\mathcal{P}_k$. We refer to aspects of the framework which speak to such events, as the *risk process* for pathogen $\mathcal{P}_k$, the details of which are described in what follows. While the description is from

the vantage point of a fixed layer j and time t, it applies to all layers $j = 1, \ldots, l$ at all times $t > 1$. At a given time t, each individual is represented as a node $v \in V^t$ within a network

$$\mathcal{D}^t \stackrel{\text{def}}{=} (x_i^t, V^t, E_j^t, A_k^t, d_j)_{i = 1, \ldots, m; j = 1, \ldots, l; k = 1, \ldots, p}$$

The set $N_j^t(v) \subseteq V^t$ represents the potential layer j risk partners for v within a fixed temporal window of duration Θ_j, i.e. during the time $[t, t + \Theta_j)$. Typically, Θ_j is related to the definition of edge relation in the survey, e.g. in SFHR, subjects were asked for the number of risk behavior partners they had in the past 30 days, so Θ_1 would be taken as 1 month.

Individual v has the propensity to sporadically engage in risk acts across layer j of their network, with a partner randomly chosen from $N_j^t(v)$. In anticipation of this, when a node v first enters the network, we assign it a propensity $t_j^R(v)$ for risk activities in layer j. This number is assumed to be time-invariant for each individual, and is randomly chosen from the positive reals using a truncated Gaussian[62] with (time-invariant) mean μ_j^R and (time-invariant) standard deviation σ_j^R. A Gaussian distribution was adopted in order to allow for controllable variation (across individuals) in the appetite for risk acts (per network layer j). The selection of $t_j^R(v)$ occurs independently for all individuals v and layers j. The quantity $t_j^R(v)/|N_j^t(v)|$ represents the expected time between successive layer j risk impulses *experienced* by v. Statistically speaking, one may say that on average, every $t_j^R(v)$ months, individual v is expected to have engaged in roughly $|N_j^t(v)| \approx d_j(v)$ risk events via layer j edges. Following previous work on the outcomes of HIV transmission in the context of unsafe sex, risk impulse streams are generated by independent Poisson processes operating at each individual v.[63,64] To achieve the above characteristics (regarding mean times between impulses) in a memoryless fashion, the time between successive risk impulses follows an exponential distribution with rate $|N_j^t(v)|/t_j^R(v)$. Upon experiencing a layer j risk impulse at time t, node v selects a partner w uniformly at random from its layer j neighbors $N_j^t(v)$, and engages in a mutual layer j risk act with w. In applications where Poisson processes are not good models of risk impulse streams, a different class of stochastic processes could be instrumented at each node, with $|N_j^t(v)|/t_j^R(v)$ serving as a parameter regulating the process' intensity.

During a layer j risk acts involving v and w, *one or more* of the pathogens $\mathcal{P}_k$ (for $k = 1, \ldots, p$) may propagate. The likelihood of this is taken to be 0 if both individuals have the same infection status, i.e. when both $v, w \notin A_k^t$ or when both $v, w \in A_k^t$. If the individuals are serodiscordant with respect to pathogen $\mathcal{P}_k$ (i.e. precisely one of them is infected), then the probability of transmission is modeled using an *infectiousness curve* $I_{j,k}$. For concreteness of exposition, let's assume v is positive for

pathogen $\mathscr{P}_k$ while w is not. The infectiousness curve $I_{j,k}$ then maps the age of v's infection (with respect to $\mathscr{P}_k$) to the probability of the pathogen's transmission during a layer j risk act. To support this within the model, it is necessary for the risk network representation to be augmented so as to maintain information about the time when individuals first become positive for each pathogen $\mathscr{P}_k$. We record this information via p functions $t_k^+ : A_k^t \rightarrow \mathbb{R}$ (for $k = 1, \ldots, p$). Finally, the susceptibility of w to becoming infected by pathogen k may be impacted by the infection status of w with respect to another pathogen $k' \in \{1, \ldots, p\}$ where $k' \neq k$. We capture this via a scalar susceptibility multiplier $\gamma_{k,k'} \in [0, +\infty)$ which amplifies or diminishes the transmission likelihood mandated by the infectiousness curve. (For simplicity, we take $\gamma_{k,k'} = 1$ whenever $k = k'$.) Aggregating these factors, we get that the probability of w becoming infected by v during a single layer j risk act involving the pair (v, w) is

$$\max\left(0, \min\left(1, \ I_{j,k}^+(t_k^+(v)) \cdot \prod_{w \in A_{k'}} \gamma_{k,k'}\right)\right)$$

While it is easy to update t_k^+ during the course of a trajectory (i.e. as previously uninfected nodes acquire the pathogen), we must also specify the infection times for individuals who were chosen to be infected at the very outset of the simulation, i.e. in the **MakePathogens** procedure (see Algorithm 3). We do this for each v in V^1 by initializing $t_k^+(v)$ to a value selected uniformly at random from the interval $[1 - T_k^+, 1]$; the values T_k^+ are new model parameters ($k = 1, \ldots, p$).

The $2l$ parameters μ_j^R and σ_j^R (for $j = 1, \ldots, l$) are added to the model, as are the p initialization parameters T_k^+ ($k = 1, \ldots, p$) and the lp infectiousness curves $I_{j,k}$ (for $j = 1, \ldots, l$ and $k = 1, \ldots, p$) that capture the time dependencies of transmission risks of pathogen $\mathscr{P}_k$ via layer j risk acts. The model is thus augmented to support the risk process via the parameters listed in Table 1.

4 Modeling network dynamism

In the next section, we extend the model to include additional parameters that specify the mechanisms governing network evolution over time, capturing the fact that:

1. An individual's risk partnerships may change if and when they decide to abandon an existing risk partner (or when the risk partner decides to abandon them). Loss of risk partners may cause individual social instability, inducing the individual to seek new risk partners. We refer to the losing and gaining risk partners as the *churn process*; it is the subject of Section 4.1.

2. The population may change because an individual enters or leaves the risk network. We refer to this as the *population process*; it is the subject of Section 4.2.

3. As individuals age over time, this may alter their risk partner preferences. We refer to this as the *aging process*; it is the subject of Section 4.3.

Each of the three processes are described below. While the narrative is written from the vantage point of a single layer j of the risk network the processes described are replicated and operate concurrently at each of the $j = 1, \ldots, l$ layers.

4.1 The churn process

While the set $N_j^t(v)$ represents the potential layer j risk partners for v at time t, it is possible for individuals to abandon (or be abandoned by) their risk partners over time. Social instability due to a loss of layer j risk partners may induce individuals to seek new risk partners to compensate for loss of social context. The central premise of our model concerning partner ''churn'' is the idea that each individual v has an ideal degree $d_j(v)$, which is the ideal size of v's ego network in layer j, based on v's stable personality. This is reflected in the fact that the ideal degree at layer j is selected using the degree distribution $\mathbb{X}_j$ in procedure **MakePopulation** (lines 8–10 of Algorithm 2). While d_j is permitted to vary over the population, here it is assumed to be fixed over time. (We note that making an individual's ideal layer-j degree d_j vary over time would not be complicated; it would simply require re-sampling the ideal degrees periodically (as per Procedure **MakePopulation**, lines 7–10). This could be implemented easily within the aging process, for example; see Section 4.3.)

On the other hand, the actual membership (and cardinality) of v's layer j risk partners $N_j^t(v)$ is permitted to vary

Table 1. Pathogen parameters.

Param.	Description	Units/range
μ_j^R	Mean time between inter layer j risk impulses	Months
σ_j^R	Inter layer j risk impulse std. dev.	Months
T_k^+	Age interval for initial $\mathscr{P}_k$ infections.	Months
$I_{j,k}^+$	Infectiousness curve for $\mathscr{P}_k$ via layer j.	Fcn. of age
$\gamma_{k,k'}$	Multiplier for susceptibility to pathogen k given prior infection by $k' \in \{1, \ldots, p\}; k' \neq k$.	Scalar

with time, albeit in a controlled fashion to be described in what follows.

Each individual v has the propensity to change the membership of $N_j^t(v)$, in an act we refer to as ''churn''. At creation time, each node v is assigned propensity for churn $t_j^C(v)$. In the current model, this number is assumed to be time-invariant for each individual, and is randomly chosen from the positive reals using a truncated Gaussian[62] with (time invariant) mean μ_j^C and (time invariant) standard deviation σ_j^C. A Gaussian distribution was used to allow for controlled variation (across individuals) in their appetite for churn acts (per network layer j). In the present model, the selection of $t_j^C(v)$ occurs independently, for all individuals v and layers j.

The quantity $t_j^C(v)/|N_j^t(v)|$ represents the mean time between successive churn impulses *experienced* by v. Statistically speaking, on average every $t_j^C(v)$ months, individual v is expected to have engaged in $|N_j^t(v)| \approx d_j(v)$ churn events at layer j. The churn impulse stream is generated by independent Poisson processes operating at each individual. To achieve the desired characteristics (regarding mean times between impulses) in a memoryless fashion, the time between successive churn impulses in the Poisson process must follow an exponential distribution with rate $|N_j^t(v)|/t_j^C(v)$.

Upon experiencing a layer j churn impulse at time t, node v engages in a Bernoulli trial, responding to the impulse by adding a partner with probability

$$p_{j+}^t(v) \overset{\text{def}}{=} \frac{\left(\frac{|N_j^t(v)| + 1}{d_j(v) + 1}\right)^{w_j^S}}{\left(\frac{|N_j^t(v)| + 1}{d_j(v) + 1}\right)^{w_j^S} + 1}$$

or abandoning an existing partner with probability $p_{j-}^t = 1 - p_{j+}^t$.

Note that $p_{j+}^t(v) = 1/2$ whenever $|N_j^t(v)| = d_j(v)$, and that

$$d_j(v) - |N_j^t(v)| \to \infty \quad \Rightarrow \quad p_{j+}^t(v) \to 1$$
$$|N_j^t(v)| - d_j(v) \to \infty \quad \Rightarrow \quad p_{j+}^t(v) \to 0$$

In short, edge loss becomes ever more likely the more actual degree exceeds ideal degree, while edge gain becomes ever more likely the more ideal degree exceeds actual degree. When ideal degree equals actual degree, edge loss and edge gain are equally likely choices in response to a churn event. The parameter w_j^S controls the rate at which $p_{j+}^t(v)$ approaches the limits asserted above, and so determines how closely individual nodes adhere to their ideal degree over the course of their network lifetimes. Justification for an individual seeking to maintain an intrinsic ideal degree comes from prior work on network ''roles'' and the correlations between role and ego network size.[51–53]

If the Bernoulli trial due to a churn impulse at v triggers abandonment of a risk partner, the partner to be abandoned is selected uniformly at random from $N_j^t(v)$. If the Bernoulli trial triggers adding a partner, the new partner is selected by calling a modified version of AddEdge in which the bias due to degree constraints has been modified (compare with line 5 of Algorithm 2) as follows:

$$a_\delta(c) := \frac{\left(\frac{|N_j^t(c)| + 1}{d_j(c) + 1}\right)^{w_j^S}}{\left(\frac{|N_j^t(c)| + 1}{d_j(c) + 1}\right)^{w_j^S} + 1}$$

Note that $a_\delta(c) = 1/2$ whenever $|N_j^t(c)| = d_j(c)$, and that

$$d_j(c) - |N_j^t(c)| \to \infty \quad \Rightarrow \quad a_\delta(c) \to 1$$
$$|N_j^t(c)| - d_j(c) \to \infty \quad \Rightarrow \quad a_\delta(c) \to 0$$

implying that a candidate c which is experiencing a layer j degree deficit is more likely to be chosen as the terminus of the new edge from v, compared to a candidate c' who is experiencing a layer j degree surplus.

The $3l$ parameters added to the model in support of the churn process are shown in Table 2.

In practice, setting the churn propensity parameters above can be tricky for modelers. Setting these parameters empirically requires data on the distribution of the duration of risk relationships. Given that subjects are more able to describe existing risk relationships than ones that have ended, the age of existing risk relationships can be used as a proxy for this. In the case study presented later, for example, we determined that risk partners were held as such for an average of 5 years (with a standard deviation 3 years). Accordingly, we took $\mu_1^C = 5.0$ and $\sigma_1^C = 3.0$; this ensured that actors chose their individual churn behavior from a distribution that allowed for a turnover (for their entire personal network) ranging from less than 2 years to 8 years or more.

4.2 The population process

The population of the risk network is controlled by both aggregate-level and individual-level processes. We refer to these respectively, as macroscopic and microscopic controls; each is treated separately below.

Table 2. Churn parameters.

Param.	Description	Units/range
μ_j^C	Layer j churn interval mean	Months
σ_j^C	Layer j churn interval std. dev.	Months
w_j^S	Layer j degree stability bias	Positive real

Macroscopic population controls. To support population growth/decline over time, we extend the dynamism model to include a new parameter r_p which captures the growth/decline of the population every 10 years (120 months). Taking $r_p = 100$, for example, indicates that the population should double every decade. Taking $r_p = -25$, on the other hand, specifies that a quarter of the population is lost every 10 years. The parameter r_p is a new addition to the model. Suppose the initial population is n_1, and the population at time t is n_t. If $r_p > 0$, the population process creates

$$V^+ \stackrel{\text{def}}{=} (1 + r_p)^{1/120} n_1 - n_t$$

new individuals in each month interval $(t, t + 1]$. If $r_p < 0$, then the population process removes

$$V^- \stackrel{\text{def}}{=} n_t - (1 - r_p)^{1/120} n_1$$

existing individuals in each month interval $(t, t + 1]$.

Microscopic population controls. In addition to the macroscopic trends in population represented by the r_p parameter, the individual agency of nodes may drive them to leave the network. Each node v has an associated "lifetime" (within the risk network), which we denote as $L(v)$ months. The value of $L(v)$ is set when node v is created (i.e. enters the risk network), and is selected by randomly drawing a positive real from a truncated distribution[62] that is the weighted sum of two Gaussians:

$$pdf(L(v) = x) = f_{tr} e^{-\sigma_{tr}(x - \mu_{tr})^2} + (1 - f_{tr}) e^{-\sigma_{st}(x - \mu_{st})^2}$$

In effect, a bimodal distribution is used to model a population consisting of two types of nodes: **transient** nodes (which occur with relative frequency f_{tr}), and **steady** nodes (which occur with relative frequency $1 - f_{tr}$). Transient nodes have lifetimes which are derived from a Gaussian distribution with mean μ_{tr} and standard deviation σ_{tr}; steady nodes have lifetimes which are derived from a Gaussian distribution with mean μ_{st} and standard deviation σ_{st}. Typically, $\mu_{st} \gg \mu_{tr}$. An individual v who was created at time $b(v)$ removes themself from all layers of the network at time $b(v) + L(v)$; v is replaced if/when mandated by the macroscopic population process described in the previous section. The parameters $\mu_{tr}, \sigma_{tr}, \mu_{st}, \sigma_{st}$ are assumed to be time-invariant, and are new additions to the model. Such a model enables one to confirm through simulation emerging understanding of the impact of episodic risk behaviors on epidemics (see Alam et al. and Zhang et al.).[65,66]

The six parameters added to the model in support of the population process, are summarized in Table 3.

Table 3. Population process parameters.

Param.	Description	Units/range
r_p	Population growth rate every 10 years	Percentage (real)
f_{tr}	Fraction that are "transient"	Between 0 and 1
μ_{tr}	Mean duration of transients' lifetimes	Months
σ_{tr}	Std. dev. of transients' lifetimes	Months
μ_{st}	Mean duration of steadies' lifetimes	Months
σ_{st}	Std. dev. of steadies' lifetimes	Months

4.3 The aging process

Each individual, when created, is assigned values for attributes x_i (for $i = 1, \ldots, m$) by random sampling from the corresponding distribution α_i. Of these attributes, some may be time dependent. In particular, if one of the x_i variables represents categorical age, then it would be incorrect for the model to assume that an individual remains the same age over the course of the network trajectory. The resulting inaccuracy is of potential consequence, since age plays a role in edge formation through the corresponding bivariate distributions $\beta_{i,j}$, which contribute to the propensities of layer j edges being created in the course of a network's evolution. It is therefore important to update any age-related attributes (from among the x_i) over time, so that they accurately change as time passes. We refer to this continuous updating of time-varying attributes as the *aging process*.

5 A case study: HIV in IDU networks

Having developed a general framework for modeling dynamic risk networks, here we apply it to network data collected in the SFHR survey, using this as a test case for the framework presented above. We are interested in the extent to which simulations within this context yield realistic approximations of what is known about historical HIV infection rates among IDU networks in New York City in the earlier years of the epidemic. Conducted between 1990 and 1993, SFHR was a cross-sectional, mixed methods project that asked 767 out-of-treatment IDUs about their risk networks and HIV risk behaviors in the prior 30 days. Interested in both individuals' network composition (namely, the presence of high-risk partners) and sociometric risk position, the SFHR study produced major findings relevant to risk populations with high HIV prevalence.[51,67–73] SFHR documented 92 connected components among 767 subjects (connected by 662 edges), including a 105-member 2-core within a large connected

Table 4. Attributes identified by ERGM

Attribute	θ	p-value
Transitive closure	3.592	***
Gender homophily (all)	0.058	0.566
Race/ethnic homophily (all)	1.205	***
Age homophily (all)	0.367	**
Number of injection partners	0.460	***
		*** ($p < 0.001$)
		** ($p < 0.01$)

component of 230 individuals. Subjects located within the 2-core were more likely to be infected with HIV,[4] causing study authors to emphasize the importance of HIV prevention within densely connected portions of the network. The SFHR study was also among the first studies of IDU communities to document network substructures and their relationship to HIV infection/transmission [74].

In the case study presented here, artificial networks of 1000, 5000, 10,000 and 25,000 nodes are generated using a model derived from the SFHR network survey, and these artificial networks are simulated over 15 year periods. We note that the risk network modeled on this data necessarily consists of just $l = 1$ layers, wherein edges represent equipment-sharing during drug co-use during the last $\Theta_1 = 30$ days. In addition, this model only considers $p = 1$ pathogens, namely $\mathscr{P}_1 = $ HIV.

As described above, ERGM analysis of the SFHR data was used to isolate actor attributes that contributed most significantly to the network topology as a whole, and produced the multivariate model for the network shown in Table 4 (see also Dombrowski et al.).[75]

Beyond the selection of attributes, the θ coefficients in the table above represent log-odds exponents that allow the weighting of model factors in the edge formation process. Thus race can be seen as $e^{1.205 - 0.460}$ (or, 2.11) times more important than number of injection partners in determining risk partners. We note here that transitive closure turned out to be the most significant factor in determining the given patterns of edge formation, followed by race/ethnic homophily, degree homophily, and age homophily. The ERGM analysis provided the value $w_1^\Delta = 3.592$ to capture the influence of triadic closure on link formation. Gender homophily—which appeared significant when examined in univariate analysis of the data—failed to be significant in the multivariate model. The remaining parameterization of the model from the SFHR study using the above attributes is presented in detail in Appendix.

The simulations in this case study share several features in common with the concurrent work of Marshall et al., who apply an ABM approach to model HIV transmission in IDU networks towards understanding the historical impact of various HIV interventions.[44] Where Marshall et al. consider just five discrete classes of individuals in constructing their networks (IDU, non-IDU, non-user MSM, non-user WSW, and the "general population"), the case study here allows edge formation to be biased in ways that reflect fine-grained pairwise distributions of gender, age, race, and the degrees of the endpoints—precisely the set of individual attributes determined by ERGM analysis to be significant influencers of edge formation likelihood. In addition, we take into account network-structural factors, in particular triadic closure, which ERGM also frequently shows to exert a significant influence on edge formation. In short, we have sought to reach beyond evident limitations which arise when "social norms and the network and individual properties that shape who forms a relationship with whom are not considered".[44:p.12] Although Marshall et al. consider the transmission of HIV via two different types of risk behavior (syringe sharing and unprotected intercourse), these risk behaviors appear to take place along edges in the same network layer. In our case study, we too consider a single pathogen (HIV) and just one network layer (where the edge relation represents injection drug equipment co-use); however, multi-layer multi-pathogen aspects of the general framework are exercised using artificial scenarios derived from this "Baseline Scenario" (see Section 5.1.3). While Marshall et al. devote considerable attention to the modeling of HIV interventions, we do not consider the topic here, choosing to calibrate our model instead on the subsaturation levels at which HIV prevalence stabilized in New York City's IDU community in the early 1990s. Most of all, for us, the case study primarily represents a realistic illustration of the expressive power of the proposed general-purpose framework for modeling multi-pathogen epidemiology on multi-layer risk networks.

5.1 Simulation experiments

Having captured the SFHR data to create a statistical network model (hereafter referred to as the HIV/IDU model), new artificial networks which follow the SFHR topology were generated, and these networks were made the subject of stochastic simulation. We note that since the mean in-network lifetimes of individuals was taken to be $\mu_{st} = 60$ months (standard deviation $\sigma_{st} = 48$ months), the total number of distinct individuals which participated in these networks over the 15 years was far greater than the number of nodes present at any given time. For example, in the 10,000 node networks, the total number of simulated network participants over the duration of the simulation was closer to $10,000 \times 180/60 = 30,000$. Given that 30,000 individual nodes participated in the network, each with an average degree of 3.4 and an average churn rate set to the duration of their participation in the network (i.e. 60 months) such that each node would on average churn through his/her entire set of connections completely over the course of their participation in the network, and so we estimate that $(30,000 \times 3.4$ initial connections) + $(30,000 \times 3.4$ churned connections) $= 204,000$ total

edge changes took place over the course of the 15 year simulation for the 10,000 node networks. Further, with a risk rate of $\mu_R = 1$ month, each of these edges was (on average) subject to a risk event monthly, from which we estimate that each simulation trial of 10,000 nodes entailed approximately 37 million risk events across which HIV infection could have taken place.

5.1.1 Validating the simulations against "ground truth". Since each simulation starts with an artificial network $\mathcal{D}'$ generated via a statistical model $\mathcal{M}(\mathcal{D})$ that is based on the SFHR dataset $\mathcal{D}$, one might ask how similar the artificial networks $\mathcal{D}'$ generated were to original SFHR network $\mathcal{D}$ from which the model $\mathcal{M}(\mathcal{D})$ was derived. According to the framework's guidelines, this similarity $\Delta(D', D)$ may be estimated via the Shannon–Jensen divergence between the corresponding constituent distributions of $\mathcal{M}(\mathcal{D})$ and $\mathcal{M}(\mathcal{D}')$, as indicated in expressions (1) and (2). Following this guideline, we conducted 10^6 independent trials, each of which generated an artificial network $\mathcal{D}'$ of size 1000. In all these trials, the artificial network always exhibited $\Delta(\mathcal{D}', \mathcal{D}) \leqslant 10^{-2}$.

Of particular interest for us was the extent to which the dynamic networks would achieve HIV-prevalence stabilization at rates known for New York City at the time.[76] In all but the smallest simulation scenario (1000 individuals), HIV prevalence in the simulations was found to stabilize at 40% and then rise very gradually thereafter over the next 15 years. This is commensurate with the history of the HIV epidemic in New York City's IDU networks during its early stages around 1990.[69,76–78] It also agrees with the ground truth of the SFHR data set itself, wherein 40% of the 767 subjects in the population sample were found to be HIV positive (50% in the 1-core, and 36% in the periphery).

To compare the quality of the artificial risk networks generated (as starting points of the simulation) to those that would be generated by an ERGM-based approach, we created 10^3 initial networks of size 10,000 using ERGM, and 10^3 using the proposed ABM procedure **MakeNetwork** given in Algorithm 1, both parameterized by statistical network data derived from the SFHR study. We then computed pairwise divergences between all 10^6 pairs of networks generated by ERGM, all 10^6 pairs of networks generated by **MakeNetwork**, and all 10^6 heterogeneous pairs of models (one generated by ERGM and the other by **MakeNetwork**). All three sets of 10^6 numbers exhibited comparable means (0.03 ± 0.005) and least upper bounds (0.1 ± 0.02). From this experiment, we concluded that the proposed ABM procedure **MakeNetwork** produces networks whose quality is commensurate to networks generated by ERGM.

Figure 1 shows the HIV prevalence (over time) in 15 year simulations of 10 independently generated networks of various sizes based on the HIV/IDU model. The bars in the graph indicate the range of findings across these 10 trials. We note that in all but the smallest of these graphs, an initial infection rate of 0.5% HIV spreads throughout the network in 12–18 months to a prevalence level of roughly 40%. From here, it remains relatively stable, rising to 50% over the next 15 years.

Figure 2 shows the number of highly infectious nodes (over time) in 15 year simulations of 10 independently generated networks based on the HIV/IDU model. All but the first of these graphs show that a surge of acute infections appears roughly 10 months into the simulation, encompassing roughly 20% of all individuals. In the 10 months after the initial spike, the acute infections dissipate, and the network returns to having relatively few acute infections (approximately 3%). This low but steady rate of new infections over time, together with the stabilization of HIV shown in Figure 1 demonstrates that while the network continues to produce new infections over time, they fail to propagate through the network, as suggested by Friedman and the original SFHR investigators.[79]

5.1.2 Continuous model validation. In the case study, we tracked the values of Δ across each simulation trajectory, finding the univariate degree distributions $\mathbb{X}$ to be the only characteristic that diverged by more than 0.0015 across the trajectory. As seen in Figure 3, the divergence of $\mathbb{X}$ distributions over the course of the trajectories remained bounded by $\Delta < 0.09$. The left graph shows the divergence of $\mathbb{X}$ as a function of time for three trials of a 1000 node dynamic network; the right graph shows the same quantity at a scale of 10,000 nodes. As can be seen, the Δ is bounded by 0.09 for both small and large networks, though larger networks exhibit less variance across trials (consistent with the wide variation shown by the 1000 node network throughout these experiments, and shown here for three trials to allow for detail that is lost in aggregating large numbers of trials).

To give the reader a sense of the extent to which $\Delta < 0.09$) acts as a control on the dynamic network, we note that in such a situation, the expected absolute value of the difference between actual and ideal degrees is 0.3 (edges). When compared to the network model's expected degree of 3.4 edges (per node), we deem this to be an acceptable level of deviation.(This deviation is understandable when one considers that nodes with very a low ideal degree (i.e. 1 or even 0, which make up approximately one-third of the total network) are consistently forced up or down by either their own or others' ''churn'' actions, resulting in a significant but predictable minority of actors who consistently are off by one from their ideal degree.) These nodes will seek to return to their ideal degree at a rate dictated by the w_j^S parameter, but at any given time, a significant number of nodes can be expected to show this
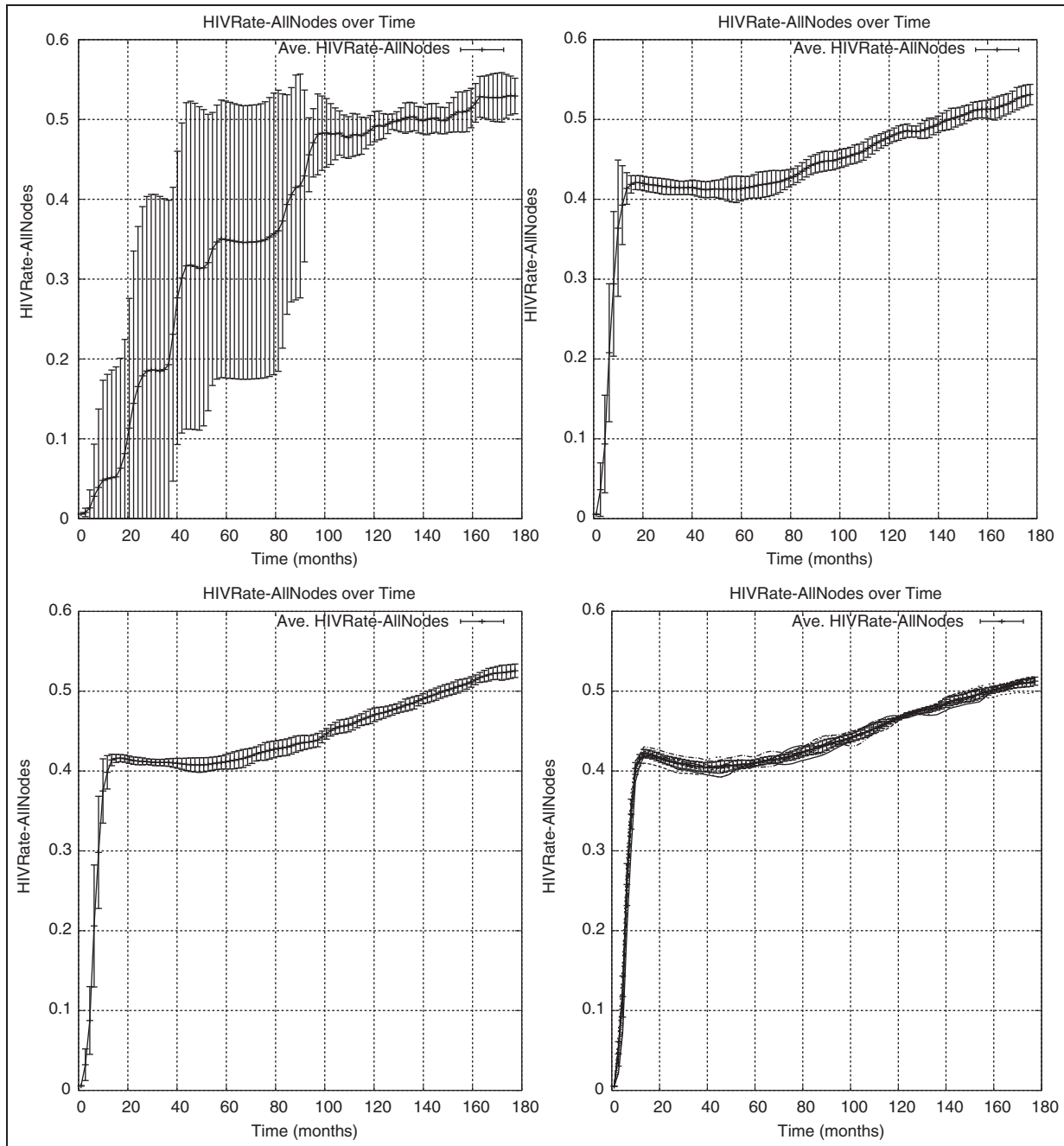
Figure 1. HIV prevalence in SFHR-based networks of size 1000, 5000, 10,000, and 25,000.

high level of variation. We note that a closer relationship between the model and the generated networks can be enforced by increasing the sociality sensitivity parameter w_j^S, which would, in turn, result in a lower Δ.

5.1.3 Experiments with derived artificial multi-layer multi-pathogen scenarios. Because our case study is based on a network model developed from the SFHR network data, which concerns the prevalence of a single pathogen (HIV)

and the structure of one risk network layer (IDU needle co-use), the case study presented so far is less comprehensive than the mathematical framework. The latter is designed to support much more general multi-layer multi-pathogen settings. To ensure that all aspects of the mathematical framework are justified and sufficiently tested, multi-layer multi-pathogen case studies are required. However, because the results of unrelated complex multi-layer multi-pathogen case studies would be difficult to
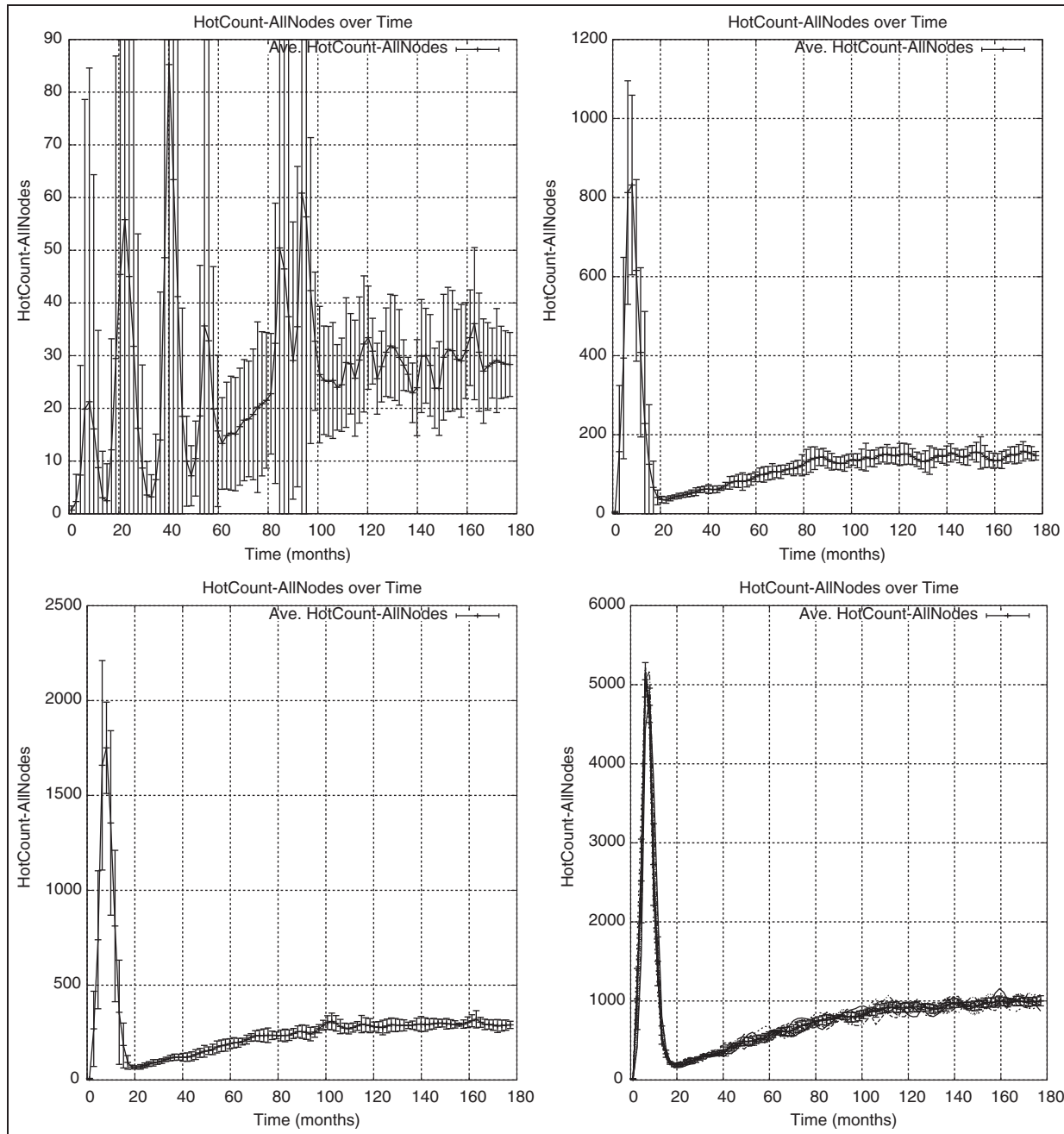
Figure 2. New HIV infections over time in networks of size 1000, 5000, 10,000, and 25,000.

validate against one another, here we consider four artificial scenarios, systematically derived from the SFHR model.

For brevity, we report only on the mean HIV rate (over 10 trials) observed in each of the four artificial scenarios, at the end of a 60 month simulation of a network of 10,000 nodes. This prevalence rate is compared with the mean rate observed in the "Base Scenario" simulations of the true SFHR network model (see Section 5.1). The artificial scenarios use the same settings as the Base Scenario, and scenarios use the same settings as the Base Scenario, and

change only very few parameters related to numbers of layers and pathogen types, as specifically indicated.

Base scenario: Here there is a single ($l = 1$) risk network layer based on the SFHR model and a single ($p = 1$) type of pathogen (HIV) which uses this network layer to propagate. As can be seen from the bottom right graph of Figure 1, the average prevalence rate of HIV in a 10,000 node network after 60 months was seen to be approximately 42%.
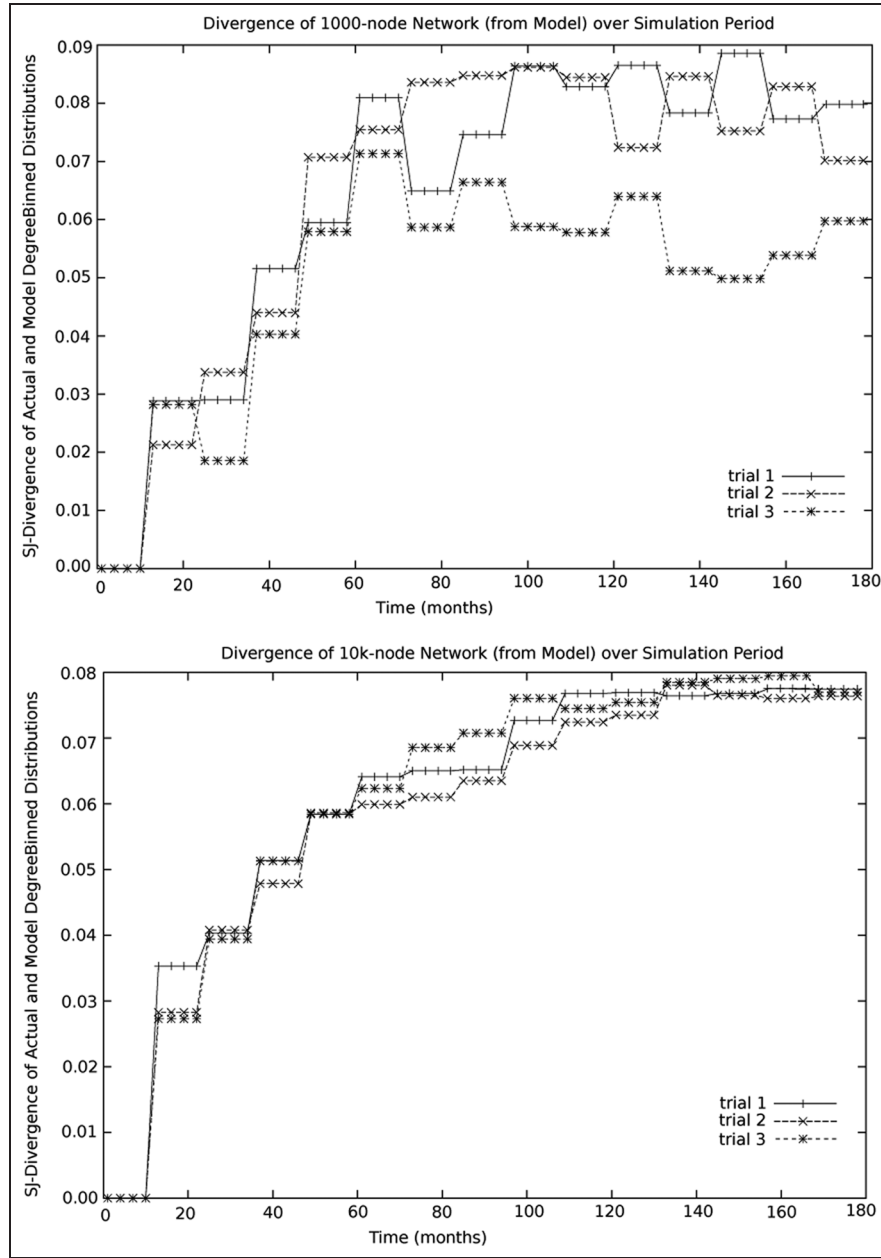
Figure 3. Divergence Δ of ℕ over 18 months for 1000 (*left*) and 10,000 (*right*) node networks on three trials.

Artificial scenario 1: Here there are multiple ($l > 1$) risk network layers each with structure based on the SFHR network model, but constructed independently of one another following procedure **MakeRelations** (see Algorithm 1). There is a single ($p = 1$) type of pathogen which behaves like HIV in terms of infectiousness curves. This pathogen simultaneously uses all $l > 1$ network layers to propagate. The mean time between risk acts in each layer is taken to be $1/l$ of the value in the Base Scenario, implying that although the pathogen uses all l layers to propagate, its rate of propagation within each layer is reduced in inverse proportion to l.

To interpret the outcomes for Artificial Scenario 1 (see Table 5), we begin by noting that in the base scenario, 42% of the population is infected, while 58% is uninfected. When the second network layer is added, an additional 28% becomes infected (that is, 48% of the previously uninfected 58%), leaving just 30% now uninfected. When the third network layer is added, an additional 11% becomes infected (that is, 36% of the previously uninfected 30%), leaving just 19% now uninfected. When the fourth network layer is added, an additional 8% becomes infected (that is, 42% of the previously uninfected 19%). Thus we observe that with each additional network layer roughly 40%

Table 5. Scenario 1: Multiple layers, one pathogen.

Number of Layers	Pathogen 1 prevalence at 60 months (%)
$l = 2$ (and $p = 1$)	70
$l = 3$ (and $p = 1$)	81
$l = 4$ (and $p = 1$)	89
Base scenario ($p = 1$ and $l = 1$)	42

Table 6. Scenario 2: Multiple pathogens, one layer.

Number of pathogens	Average prevalence at 60 months (across all p pathogens) (%)	Ave. pairwise correlation of pathogen occurrence
$p = 2$ (and $l = 1$)	42	0.86
$p = 3$ (and $l = 1$)	43	0.76
$p = 4$ (and $l = 1$)	44	0.72
Base scenario ($p = 1$ and $l = 1$)	42	

(between 36% and 48%) of the previously uninfected nodes become reachable by the pathogen. This is expected, since each of the network layers is structured independently, and with just one layer, roughly 40% of the network was infected. Slowing down the risk act rate does not retard pathogen transmission because even with four layers and each layer operating at one-quarter of the base scenario's risk rate, we expect the pathogen's progress through each layer to be comparable to what is experienced in the base scenario at month $60/4 = 15$—but as the bottom right graph of Figure 1 shows, the Base Scenario has already stabilized to roughly 40% prevalence by month 15.

Artificial scenario 2: Here there is a single ($l = 1$) risk network layer with structure based on the SFHR network model. There are multiple ($p > 1$) types of pathogens, all of which individually behave like HIV, but must share the single risk network layer to propagate. Cross-pathogen susceptibility multipliers $\gamma_{k,k'}$ are all taken as 1, meaning that prior infection by k' neither enhances nor reduces susceptibility to pathogen k ($k \neq k'$). The mean time between risk acts in the layer is taken to be the same as that in the base scenario, meaning that every time a risk event occurs between two vertices, upto $p > 1$ types of pathogens may be simultaneously and independently transmitted between the two parties.

Scenario 2 (see Table 6) show that all pathogens reach roughly the same prevalence levels in 60 months as was manifested in the base scenario. Also listed is the correlation coefficient $r(k, k')$ between infection status for pathogen k versus k' (for $k \neq k'$); we see that the average value of the correlation (across all distinct pairs k, k') is quite high (though it decreases slightly as the number of pathogens increases). This indicates that network structural features are at play which cause "clumping" of all pathogen infections (independent of type).

Artificial scenario 3: Here there are multiple ($l > 1$) risk network layers each with structure based on the SFHR network model, but constructed independently of one another following procedure **MakeRelations** (see Algorithm 1). There are multiple ($p > 1$) types of pathogens, all of which individually behave like HIV, but with each having its own dedicated mode of propagation (embodied in a separate risk network layer); i.e. $p = l$. Cross-pathogen susceptability multipliers $\gamma_{k,k'}$ are all taken as 1, meaning that

Table 7. Scenario 3: Multiple layers, multiple non-interacting pathogens.

Number of pathogens p Number of layers l	Average prevalence at 60 months (across all p pathogens) (%)	Ave. pairwise correlation of pathogen occurrence
$p = l = 2$	42	0.12
$p = l = 3$	43	−0.11
$p = l = 4$	42	0.08
Base scenario ($p = l = 1$)	42	

prior infection by k' neither enhances nor reduces susceptibility to pathogen k ($k \neq k'$). The mean time between risk acts for each layer is taken to be the same as that in the base scenario. Since each risk event occurs in a layer, and each layer is devoted to a single pathogen type, when a risk event occurs between two vertices, at most one type of pathogen may be transmitted. However, since all $l = p$ layers are operating independently, all p pathogens propagate concurrently through the population, albeit with each pathogen making use of its own dedicated risk network layer.

The outcomes for Artificial Scenario 3 (see Table 7) show that all pathogens reach roughly the same prevalence levels in 60 months as was observed in the base scenario. However, in examining the correlation $r(k, k')$ between infection status for pathogen k versus k' (for $k \neq k'$), we see that the average value of the correlation (across all distinct pairs k, k') is now quite low. This indicates that shared network structural features that were at play in Artificial Scenario 2 are disrupted when the pathogens are forced to travel across multiple independently constructed risk network layers.

Artificial Scenario 4: This scenario is identical to scenario 3, except that cross-pathogen susceptibility multipliers $\gamma_{k,k'}$ are all taken as 0. This means that prior infection by pathogen k' makes an individual immune to pathogen k ($k \neq k'$).

The outcomes for Artificial Scenario 4 (see Table 8) show that the pathogens *considered collectively*, reach roughly the same prevalence levels in 60 months as was observed in the base scenario. That is, $2 \times 21\% \approx 3 \times 15\% \approx 4 \times 12\%$

Table 8. Scenario 4: Multiple layers, multiple interacting pathogens.

Number of Pathogens p Number of Layers l	Average prevalence at 60 months (across all p pathogens)(%)
$p = l = 2$	22
$p = l = 3$	15
$p = l = 4$	12
Base Scenario ($p = l = 1$)	42

$\approx 42\%$. This is expected, since cross-pathogen susceptibility multipliers force the p pathogens to share host infection opportunities between them.

Taken together, these four artificial scenarios, and the plausible explanations for the outcomes observed in each of them, provide us with a measure of confidence in our framework's general applicability to epidemiological modeling involving multi-pathogen multi-layer risk networks.

6 Conclusions

Simulations of artificial risk networks generated by the HIV/IDU model exhibited stabilization of HIV prevalence to sub-saturation levels similar to those observed historically in IDU networks in New York City during the early stages of the HIV epidemic.[69,76–78] Simulations in which the virulence of the pathogen was raised (modeled as an overall increase in the likelihood of transmission in any given risk event) showed little change to overall stabilization levels for networks of 5000 $+$ nodes—a truly counterintuitive finding, given that so much public health effort is directed to lowering individual risk in stemming the spread of HIV. Of interest is that stabilization manifests in networks of 5000 to 25,000 nodes, but is not clear in smaller networks; the 1000 node network shows little evidence of HIV stabilization, and a wide range of prevalence rates at any given time when examined across independent simulation trials. The framework developed here was able to reveal historical HIV prevalence trajectories through the simulation of dynamic risk networks which reflected *both known (micro) IDU behavioral profiles and (macro) structural characteristics of a real-world risk network*, as recorded in the SFHR survey; as such, it represents a significant step forward in our ability to model and simulate the dynamics of infectious disease.

More generally, we note that while traditional social network research continues to produce considerable data on infection profiles, and equally detailed data on the broad demographic and behavioral profiles of at-risk communities and their risk behaviors, such research has not—and for reasons of cost often cannot—produce long-term, dynamic data on these same populations. At best, it provides snapshots of social processes within risk networks that are otherwise known to be in a state of flux. The general framework presented here—demonstrated through a real case study of HIV in IDU networks—shows that simulation provides an opportunity to understand the long-term dynamics of risk networks themselves. Looking to the future, the framework opens the door to understanding how the specific patterns of risk-bearing relationships came to be the way they are, how infections move (and do not move) across these topologies, where risk networks and the infections they contain are going in the future, and what the impacts of various interventions might be.

References

1. Goforth RRR and Berleant D. A simulation model to assist in managing the HIV epidemic: IMAP2. *Simulation* 1994; 63(2):128–136.
2. Bell DC, Montoya ID, Atkinson JS, et al. Social networks and forecasting the spread of HIV infection. *JAIDS—J Acq Imm Def* 2002; 31(2): 218–229.
3. Goodreau SM. Assessing the effects of human mixing patterns on human immunodeficiency virus-1 interhost phylogenetics through social network simulation. *Genetics* 2006; 172(4): 2033.
4. Friedman SR, Neaigus A, Jose B, et al. Sociometric risk networks and risk for HIV infection. *Am J Pub Health* 1997; 87(8): 1289–1296.
5. Bachanas PJ, Morris MK, Lewis-Gess JK, et al. Predictors of risky sexual behavior in african american adolescent girls: Implications for prevention interventions. *J Pediatr Psychol* 2002; 27(6): 519–530.
6. Hsieh JL, Sun CT, Kao GYM, et al. Teaching through simulation: Epidemic dynamics and public health policies. *Simulation* 2006; 82(11): 731–759.

7. Friedman SR. *Social Networks, Drug Injectors' Lives, and HIV/AIDS*. New York: Springer, 1999.

8. Nikolai C and Madey G. Tools of the trade: A survey of various agent based modeling platforms. *JASSS—J Artif Soc S* 2009; 12(2): 2.

9. Bian L. A conceptual framework for an individual-based spatially explicit epidemiological model. *Environment and Planning B Planning and Design* 2004; 31(3): 381–395.

10. Dunham JB. An agent-based spatially explicit epidemiological model in MASON. *JASSS—J Artif Soc S* 2005; 9(1): 3.

11. Lopez-Paredes A, Edmonds B and Klugl F. Special issue: Agent based simulation of complex social systems. *Simulation* 2012; 88(1): 4–6.

12. Luke S, Cioffi-Revilla C, Panait L, et al. MASON: A multiagent simulation environment. *Simulation* 2005; 81(7): 517–527.

13. Stroud P, Del Valle S, Sydoriak S, et al. Spatial dynamics of pandemic influenza in a massive artificial society. *JASSS—J Artif Soc S* 2007; 10(4): 9.

14. Bagni R, Berchi R and Cariello P. A comparison of simulation models applied to epidemics. *JASSS—J Artif Soc S* 2002; 5(3): 1–23.

15. Eidelson BM and Lustick I. VIR-POX: An agent-based analysis of smallpox preparedness and response policy. *JASSS—J Artif Soc S* 2004; 77(3). http://jasss.soc.surrey.ac.uk/7/3/6.html. Accessed March 17, 2014.

16. Huang CY, Sun CT, Hsieh JL, et al. Simulating SARS: Small-world epidemiological modeling and public health policy assessments. *JASSS—J Artif Soc S* 2004; 7: 100–131.

17. Yoneyama T and Krishnamoorthy MS. Simulating the spread of influenza pandemic of 2009 considering international traffic. *Simulation* 2012; 88(4): 437–449.

18. Dunn AG and Gallego B. Diffusion of competing innovations: The effects of network structure on the provision of healthcare. *JASSS—J Artif Soc S* 2010; 13(4): 8.

19. Huang CY, Tsai YS and Wen TH. A network-based simulation architecture for studying epidemic dynamics. *Simulation* 2010; 86(5–6): 351–368.

20. Huang CY, Sun CT, Hsieh JL, et al. A novel small-world model: Using social mirror identities for epidemic simulations. *Simulation* 2005; 81(10): 671–699.

21. Huang CY, Tsai YS, Sun CT, et al. Influences of resource limitations and transmission costs on epidemic simulations and critical thresholds in scale-free networks. *Simulation* 2009; 85(3): 205–219.

22. Hamill L and Gilbert N. Social circles: A simple structure for agent-based social network models. *JASSS—J Artif Soc S* 2009; 12(2): 3.

23. Watts DJ and Strogatz SH. Collective dynamics of ''small-world'' networks. *Nature* 1998; 393: 440–442.

24. Barabasi AL and Albert R. Emergence of scaling in random networks. *Science* 1999; 286(5439): 509–512.

25. Dorogovtsev SN and Mendes JFF. *Evolution of Networks: From Biological Nets to the Internet and WWW*. New York: Oxford University Press, 2003.

26. Bender EA and Canfield ER. The asymptotic number of labeled graphs with given degree sequences. *J Combin Theory A*. 1978; 24(3): 296–307.

27. McKay BD and Wormald NC. Asymptotic enumeration by degree sequence of graphs of high degree. *Eur J Comb* 1990; 11: 565–580.

28. Bollobás B. The distribution of the maximum degree of a random graph. *Discrete Math* 1980; 32(2): 201–203.

29. Bollobás B. *Random Graphs*. Cambridge: Cambridge University Press, 2001.

30. Bollobás B and Riordan O. Random graphs and branching processes. In:Bollobs B, Kozma R, Mikls D, et al. (eds) Handbook of Large-Scale Random Networks (*Bolyai Society Mathematical Studies*, Vol. 18). Berlin; Heidelberg, Germany: Springer, 2008, pp.15–115.

31. Bayati M, Kim J and Saberi A. A sequential algorithm for generating random graphs. *Algorithmica* 2010; 58: 860–910.

32. Blitzstein J and Diaconis P. A sequential importance sampling algorithm for generating random graphs with prescribed degrees. *Internet Mathematics* 2011; 6(4): 489–522.

33. Chatterjee S, Diaconis P and Sly A. Random graphs with a given degree sequence. *Ann Appl Probab* 2011; 21(4): 1400–1435.

34. Stanton I and Pinar A. Sampling graphs with a prescribed joint degree distribution using Markov chains. In: *Proceedings of SIAM workshop on Algorithm Engineering and Experiemtns (ALENEX)*, San Francisco, CA, 22 January 2011, pp.151–163.

35. Holland PW and Leinhardt S. An exponential family of probability distributions for directed graphs. *J Am Stat Assoc* 1981; 76(373): 33–50.

36. Frank O and Strauss D. Markov graphs. *J Am Stat Assoc* 1986; 81(395): 832–842.

37. Snijders TA, Pattison P, Robins G, et al. New specifications for exponential random graph models. *Sociol Methodol* 2006; 36: 99–153.

38. Goodreau SM. Advances in exponential random graph (*p**) models applied to a large social network. *Social Networks* 2007; 29(2): 231–248.

39. Goodreau SM, Kitts JA and Morris M. Birds of a feather, or friend of a friend? Using exponential random graph models to investigate adolescent social networks. *Demography* 2009; 46(1): 103–125.

40. Kolaczyk ED. *Statistical Analysis of Network Data: Methods and Models*. Softcover reprint of hardcover 1st edition. New York; London: Springer, 2010.

41. Lieberman S. Extensible software for whole of society modeling: Framework and preliminary results. *Simulation* 2012; 88(5): 557–564.

42. Goodreau SM. A decade of modelling research yields considerable evidence for the importance of concurrency: A response to Sawers and Stillwaggon. *J Int AIDS Soc* 2011; 14: 12.

43. Snijders TA, Van de, Bunt GG and Steglich CE. Introduction to stochastic actor-based models for network dynamics. *Social Networks* 2010; 32(1): 44–60.

44. Marshall BDL, Paczkowski MM, Seemann L, et al. A complex systems approach to evaluate HIV prevention in metropolitan areas: Preliminary implications for combination intervention strategies. *PLoS ONE* 2012; 7(9): e44833.

45. Stroele V, Oliveira J, Zimbrao G, et al. Mining and analyzing multirelational social networks. In: *Proceedings of international conference on computational science and engineering CSE '09*, Vancouver, Canader, 29–31 August 2009, Vol. 4, pp.711–716.

46. Rodriguez MA and Shinavier J. Exposing multi-relational networks to single-relational network analysis algorithms. *Journal of Informetrics* 2010; 4(1): 29–41.

47. Ströele V, Zimbrão G and Souza JM. Group and link analysis of multi-relational scientific social networks. *J Syst Softw* 2013; 86(7): 1819–1830.

48. Szell M, Lambiotte R and Thurner S. Multirelational organization of large-scale social networks in an online world. *Proceedings of the National Academy of Sciences* 2010; 107(31): 13636–13641.

49. Zhao K, Yen J, Ngamassi LM, et al. Simulating inter-organizational collaboration network: A multi-relational and event-based approach. *Simulation* 2012; 88(5): 617–633.

50. Bearman PS, Moody J and Stovel K. Chains of affection: The Structure of adolescent romantic and sexual networks. *Am J Sociol* 2004; 110(1): 44–91.

51. Friedman SR, Furst RT, Jose B, et al. Drug scene roles and HIV risk. *Addiction* 1998; 93(9): 1403–1416.

52. Curtis R, Friedman SR, Neaigus A, et al. Street-level drug markets: Network structure and HIV risk. *Social Networks* 1995; 17(3–4): 229–249. Social networks and infectious disease: HIV/AIDS. Available from: http://www.sciencedirect.com/science/article/pii/037887339500264O.

53. Romero-Severson EO, Alam SJ, Volz EM, et al. Heterogeneity in number and type of sexual contacts in a gay urban cohort. *Stat Comm Infect Diseases* 2012; 4. http://dx.doi.org/10.1515/1948-4690.1042. Accessed March 17, 2014.

54. Barla A, Odone F and Verri A. Histogram intersection kernel for image classification. In: *Proceedings of the international conference on image processing*, Barcelona, Spain, 14–18 September 2003, Vol. 3, pp.513–516.

55. Read CB. Freeman–Tukey chi-squared goodness-of-fit statistics. *Stat Prob Let* 1993; 18(4): 271–278.

56. Stephens MA. EDF statistics for goodness of fit and some comparisons. *J Am Stat Assoc* 1974; 69(347): 730–737.

57. Kullback S and Leibler RA. On information and sufficiency. *Ann Math Stat* 1951; 22(1): 79–86.

58. Endres DM and Schindelin JE. A new metric for probability distributions. *IEEE Trans Inform Theory* 2003; 49(7): 1858–1860.

59. Österreicher F and Vajda I. A new class of metric divergences on probability spaces and its applicability in statistics. *Ann I Stat Math* 2003; 55(3): 639–653.

60. Bharathy GK and Silverman B. Holistically evaluating agent-based social systems models: A case study. *Simulation* 2013; 89(1): 102–135.

61. Robert CP and Casella G. *Monte Carlo Statistical Methods (Springer Texts in Statistics)*. Secaucus, NJ: Springer-Verlag, 2005.

62. Robert CP. Simulation of truncated normal variables. *Stat Comput* 1995; 5: 121–125.

63. Barta WD, Tennen H and Kiene SM. Alcohol-involved sexual risk behavior among heavy drinkers living with HIV/AIDS: Negative affect, self-efficacy, and sexual craving. *Psychol Addict Behav* 2010; 24(4): 563–570.

64. Xia Y, Morrison-Beedy D, Ma J, et al. Modeling count outcomes from HIV risk reduction interventions: A comparison of competing statistical models for count responses. *AIDS Research and Treatment* 2012; doi:10.1155/2012/593569. http://www.hindawi.com/journals/art/2012/593569/.

65. Alam SJ, Zhang X, Romero-Severson EO, et al. Detectable signals of episodic risk effects on acute HIV transmission: Strategies for analyzing transmission systems using genetic data. *Epidemics* 2013; 5(1): 44–55. doi: 10.1016/j.epidem.2012.11.003.

66. Zhang X, Zhong L, Romero-Severson E, et al. Episodic HIV risk behavior can greatly amplify HIV prevalence and the fraction of transmissions from acute HIV infection. *Stat Comm Infect Diseases* 2012; 4: 1041. doi: 10.1515/1948-4690.1041. http://www.ncbi.nlm.nih.gov/pmc/articles/PMC3778933/.

67. Friedman SR, Mateu-Gelabert P, Curtis R, et al. Social capital or networks, negotiations, and norms? A neighborhood case study. *Am J of Prevent Med* 2007; 32(6 Suppl): S160–170.

68. Goldstein M, Friedman SR, Neaigus A, et al. Self-reports of HIV risk behavior by injecting drug users: Are they reliable? *Addiction* 1995; 90(8): 1097–1104.

69. Des Jarlais DC, Perlis T, Friedman SR, et al. Declining seroprevalence in a very large HIV epidemic: Injecting drug users in New York City, 1991 to 1996. *Am J Pub Health* 1998 Dec; 88(12): 1801–1806.

70. Jose B, Friedman SR, Neaigus A, et al. Syringe-mediated drug-sharing (backloading): A new risk factor for HIV among injecting drug users. *AIDS* 1993; 7(12): 1653–1660.

71. Kottiri BJ, Friedman SR, Neaigus A, Curtis R and Des Jarlais DC. Risk networks and racial/ethnic differences in the prevalence of HIV infection among injection drug users. *JAIDS—J Acq Imm Def* 2002; 30(1): 95–104.

72. Neaigus A, Friedman SR, Curtis R, et al. The relevance of drug injectors' social and risk networks for understanding and preventing HIV infection. *Soc Sci Med* 1994; 38(1): 67–78.

73. Neaigus A, Friedman SR, Goldstein M, et al. Using dyadic data for a network analysis of HIV infection and risk behaviors among injecting drug users. *NIDA Res Mg* 1995; 151: 20–37.

74. Friedman SR, Curtis R, Neaigus A, et al. *Social Networks, Drug Injectors' Lives, and HIV/AIDS*. New York: Kluwer Academics, 1999.

75. Dombrowski K, Khan B, McLean K, et al. A re-examination of connectivity trends via exponential random graph modeling in two IDU risk networks. *Substance Use and Misuse* 2013; 48(14): 1485–1497.

76. Des Jarlais DC, Arasteh K and Friedman SR. HIV among drug users at Beth Israel Medical Center, New York City, the first 25 years. *Subst Use Misuse* 2011; 46(2–3): 131–139.

77. Des Jarlais DC, Perlis T, Arasteh K, et al. HIV incidence among injection drug users in New York City, 1990 to 2002: Use of serologic test algorithm to assess expansion of HIV prevention services. *Am J Pub Health* 2005; 95(8): 1439–1444.

78. Des Jarlais DC, Friedman SR, Novick DM, et al. et al. HIV-1 infection among intravenous drug users in manhattan, New York City, from 1977 through 1987. *JAMA: J Am Med Assoc* 1989; 261(7): 1008–1012.

79. Friedman SR, Kottiri BJ, Neaigus A, et al. Network-related mechanisms may help explain long-term HIV-1 seroprevalence levels that remain high but do not approach population-group saturation. *Am J Epidemiology* 2000; 152(10): 913–922.

80. Dombrowski K, Khan B, McLean K, et al. A re-examination of connectivity trends via exponential random graph modeling in two IDU risk networks. *Subst Use Misuse* 2013; 48(14): 1485–1497. doi: 10.3109/10826084.2013.796987.

81. Cates W, Chesney MA and Cohen MS. Primary HIV infection—A public health opportunity. *Am J Pub Health* 1997; 87(12): 1928–1930.

82. Kahn JO and Walker BD. Acute human immunodeficiency virus type 1 infection. *New Engl J Med* 1998; 339(1): 33–39.

83. Lyles CM, Kay LS, Crepaz N, et al. Best-evidence interventions: Findings from a systematic review of HIV behavioral interventions for US populations at high risk, 2000–2004. *Am J Pub Health* 2007; 97(1): 133–143.

84. Hagan Thiede H, Weiss NS, et al. Sharing of drug preparation equipment as a risk factor for hepatitis C. *Am J Pub Health* 2001; 91(1): 42–46.

85. Daar ES, Moudgil T, Meyer RD, et al. Transient high levels of viremia in patients with primary human immunodeficiency virus type 1 infection. *New Engl J Med* 1991; 324(14): 961–964.

Author biographies

Bilal Khan is professor of mathematics and computer science at City University of New York, John Jay College.

Kirk Dombrowski is professor of sociology at University of Nebraska–Lincoln.

Mohamed Saad is research staff at the Social Network Research Group (snrg-nyc.org) and Chief Scientist at Microjan Inc.

Appendix. Model parameterizations

The following parameters were taken from the SFHR data and used in the case study above:

A.1 Static network

In the context of this work, by applying ERGM analysis to the risk network $\mathcal{D}$ obtained from the SFHR survey data, we determined that $m = 4$ individual attributes exerted significant influence on the likelihood of edge formation. The names and categorical ranges of each of these significant attributes $X = \{x_1, \ldots x_4\}$ are tabulated in Table 9; a full exposition of their derivation by ERGM analysis is available.[80] The univariate (resp. bivariate) distributions of

Table 9. Significant attributes (as determined by ERGM).

Name	Possible values (U_i)
x_1 : Gender	{Male, Female}
x_2 : Ethnicity	{White, Hispanic, African American, Other}
x_3 : AgeBinned	{[15–20), [20–25), [25–30), [30–35), [35–40), [40–45), [45–50), [50–55)}
x_4 : DegreeBinned	{[0–2), [2–4), [4–10), [10–20)}

Table 10. Gender univariate α_1.

	Male	Female
α_1	540/767	227/767

Table 11. Ethnicity univariate α_2.

	White	Hispanic	African American	Other
α_2	243/767	206/767	311/767	7/767

Gender, Ethnicity, AgeBinned, and DegreeBinned are tabulated in Tables 10–13 (resp. Tables 14–17). Finally, as 39% of individuals in the SFHR risk network were HIV +, in the corresponding statistical network model we take $p = 0.39$.

A.2 Pathogen model for HIV/IDU

Inter risk impulse interval mean μ_R was set in accordance with the SFHR data set. Given that the criteria for connection in the SFHR survey was "a risk event in the last 30 days", :p.115 the risk parameter μ_R was set to 1.0 months, so that nodes would draw from a distribution of risk profiles centered at 1 risk event per month per risk partner. With a mean degree of 3.4, this means, in effect, that the average actor will engage 3–4 risk events in a 30 day period. Further description in the SFHR documentation points to a wide range of risk behavior rates. SFHR interview subjects reported an average of 112 monthly injections (not all of which, obviously, involved a risk event), with a standard deviation of 139.[7:p.120] Taking the latter as our guide, we set the **inter risk impulse interval standard deviation** σ_R to 1.0 months, such that the variation in risk was roughly equal to the overall rate. This produced a truncated distribution with a near flat distribution between 0 and 2, and long but diminishing tail for rates greater than 2 risk events per number of risk partners per month.

In the case of HIV, the infectiousness curve can be approximated as a function of infection age that decreases

Table 12. AgeBinned univariate α_3.

	[15–20)	[20–25)	[25–30)	[30–35)	[35–40)	[40–45)	[45–50)	[50–55)
α_3	6/767	32/767	158/767	172/767	198/767	159/767	23/767	19/767

Table 13. DegreeBinned univariate χ.

	[0–2)	[2–4)	[4–10)	[10–20)
χ	322/767	221/767	161/767	63/767

Table 14. Gender bivariate β_1.

β_1	Male	Female
Male	94/145	51/145
Female	76/127	51/127

Table 15. Ethnicity bivariate β_2.

β_2	White	Hispanic	African Am.	Other
White	115/178	18/178	43/178	2/178
Black	11/157	112/157	31/157	3/157
Hispanic	32/175	25/175	117/175	1/175
Other	2/7	4/7	1/7	0

sharply at approximately 3 months, and remains at low levels until approximately 8 years later.[81–83] We use this information to construct two-parameter infectiousness function $I_{j,1}$ shown in Figure 4. Given that we know the infectiousness drop sharply approximately 3 months after the time of initial infection, we approximate the infectiousness curve $I_{j,1}$ by a step function whose value is p_j^H for the 3 month high infectiousness, or "acute" phase, and $c_j^{L/H} \cdot p_j^H$ thereafter, in the low infectiousness or "chronic" phase. We note here that $c_j^{L/H} \ll 1$. With such a model, if $t - t_1^+(v) \leqslant 3$ then with probability p_j^H individual w acquires HIV from v during the layer j risk act. If, on the other hand, $t - t_1^+(v) > 3$, then the transmission occurs with a much smaller probability $c_j^{L/H} \cdot p_j^H$. In either case,

if w acquires HIV during the layer j risk act, then w is added to A_1^t and we set its infection time $t_1^+(w) := t$. To support such a model of HIV pathogen transmission, the two parameters p_1^H and $c_1^{L/H}$ must be specified.

The **infection probability in infectious period** p_H was initially intended as a tuning parameter such that, once the other parameters had been set according to the SFHR data, a series of trials could be undertaken in simulated networks and the transmission parameter set such that the simulated HIV rates for the SFHR settings regularly matched those of the SFHR sample (i.e. 40%). This proved unnecessarily complex, as variations in the infectiousness probability had little effect on the overall HIV rates. In the end, we used a mean rate of risk for equipment co-use during periods of high infectiousness of 5% chance of infection per risk event. Rates at low as 2% and as high as 10% showed only small effect in overall infection rates. While no precise data are available for HIV per-event risk rates, colleagues Hagan et al. found that HCV risk among IDU showed a three- to five-fold increase in seroconversion rates and a risk factor of 5.9 for those who shared drug preparation equipment or syringes.[84]

The **reduction in infectiousness post 3 months** $c_{L/H}$, was taken to be 1/100, as an estimate for a wide range of published measures, from 1/20th to 1/1000th, based on comparisons between periods of high and low infectiousness.[82,85]

The **infection interval** T_+ **for individuals initially HIV** $+$ was taken to be three weeks, as an approximation for published a range of estimates from 9 to 14 weeks.[82,85]

A.3 Network dynamism model for HIV/IDU

The rate at which network actors changed their current list of risk partners **churn interval mean** μ_C was taken to

Table 16. AgeBinned bivariate β_3.

β_3	[15–20)	[20–25)	[25–30)	[30–35)	[35–40)	[40–45)	[45–50)	[50–55)
[15–20)	1/4	1/4	2/4	0	0	0	0	0
[20–25)	1/26	1/26	7/26	6/26	7/26	3/26	1/26	0
[25–30)	1/147	8/147	41/147	45/147	38/147	12/147	2/147	0
[30–35)	0	5/153	33/153	50/153	43/153	16/153	5/153	1/153
[35–40)	0	4/161	20/161	41/161	56/161	29/161	6/161	5/161
[40–45)	0	2/137	14/137	27/137	44/137	40/137	3/137	7/137
[45–50)	0	0	2/20	6/20	6/20	4/20	2/20	0
[50–55)	0	0	0	2/14	6/14	4/14	0	2/14

Table 17. DegreeBinned bivariate $\bar{\bar{\chi}}$.

$\bar{\bar{\chi}}$	[0–2)	[2–4)	[4–10)	[10–20)
[0–2)	77/158	37/158	29/158	15/158
[2–4)	57/203	77/203	40/203	29/203
[4–10)	42/195	50/195	64/195	39/195
[10–20)	15/100	23/100	31/100	31/100
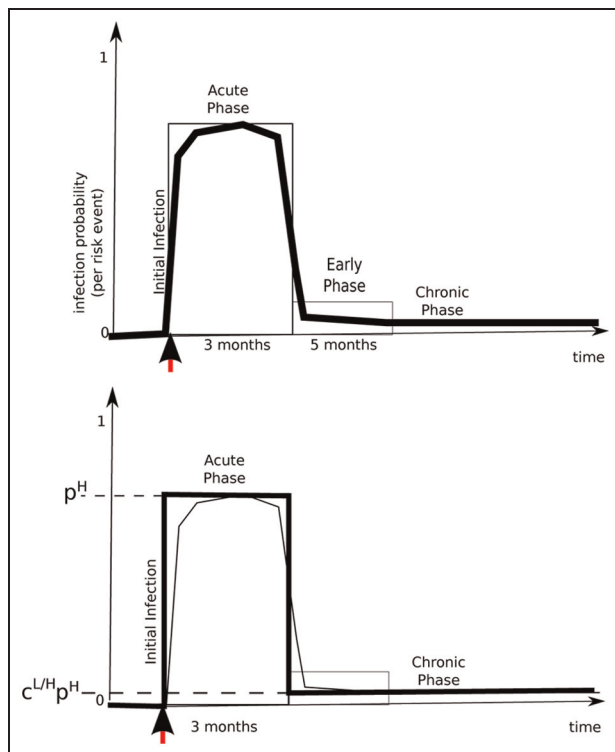
Figure 4. (*Top*) Infectiousness of HIV as a function of age of infection; (*bottom*) a simplified two-parameter representation.

reflect a network wherein risk partners are held as such for an average of 5 years. Justification for this includes the fact that 53 percent of the network noted that they had known *all* of their network for at least a year, and 43 percent of the network felt "very close" to some or all of their network.[7:p.130] Ethnographic reports from the SFHR network note considerable longevity to risk partnerships (see also Friedman, Chapter 3).[7,52] Here again, where wide variation in individual characteristics were obtained, we set the **churn interval standard deviation** $\sigma_C = 3.0$ years to ensure that actors chose their individual churn behavior from a distribution that allowed for rapid turn overs of less than 2 years (for their entire personal network) to long-term partnerships (of 8 years or more). It was later

discovered that the changes to μ_C and σ_C had little effect on the simulation outcomes with respect to asymptotic HIV rates.

The **degree stability bias** w_S determined how closely individual nodes maintained their degree over the course of their participation in the network. On the whole, the justification for a fixed degree comes from prior work on drug scene "roles".[51,52] While, obviously, no direct parameter settings can be drawn from the data described by Friedman et al. and Curtis et al., the function used to determine the effects of the parameter, and the original parameter setting of 2.9 was designed such that variations from initial degree by roughly 30% were very likely to be corrected. It was discovered that the changes to w_S had little effect on the simulation outcomes with respect to asymptotic HIV rates.

The macroscopic population process **growth rate** $r_P = 0$ was set thereby specifying a constant population size, although certainly individuals were leaving and entering throughout (see below).

While a number of individuals in the SFHR study had few partners, or would be considered marginal members of the network itself, there is also a wealth of ethnographic reports on very short-term visitors to the network.[51,52] As far as we know, no solid estimates of the proportion of these transient participants is given, nor would we expect the number to be uniform across sub-networks in New York City. A "drug market" zone like that studied by the SFHR project is likely to have a greater proportion of transient members than a smaller, less public network. We took the **fraction of individuals that are "transient"** $f_{tr} = 0$, as a base-line in the simulations here.

As with network churn, a dearth of diachronic data meant that we relied heavily for these parameter settings on ethnographic observation and the experience of project co-authors in the SFHR network. While many of the SFHR network members had been injectors for longer than 9 years, this does not mean that they participated in the same IDU network for that entire time. For this reason, the settings were made identical to the churn settings above, **mean duration of steadies' lifetimes** $\mu_{st} = 5.0$ years, and **standard deviation of steadies' lifetimes** $\sigma_{st} = 3.0$ years, so that participation varied widely from 2–8 years for "steady" participants.